

to appear in the June 2000 issue of the Astronomical Journal

## Extremely Red Objects in the Field of QSO 1213–0017: A Galaxy Concentration at $z = 1.31^{1,2}$

MICHAEL C. LIU

*Department of Astronomy, University of California, Berkeley, CA 94720*

[mliu@astro.berkeley.edu](mailto:mliu@astro.berkeley.edu)

ARJUN DEY<sup>3</sup>

*National Optical Astronomy Observatories, Tucson, AZ 85719*

JAMES R. GRAHAM AND KEVIN A. BUNDY

*Department of Astronomy, University of California, Berkeley, CA 94720*

CHARLES C. STEIDEL<sup>4</sup> AND KURT ADELBERGER

*Palomar Observatory, Caltech 105-24, Pasadena, CA 91125*

MARK E. DICKINSON

*Space Telescope Science Institute, 3700 San Martin Drive, Baltimore, MD 21218*

### ABSTRACT

We have discovered a concentration of extremely red objects (EROs;  $R - K > 6$ ) in the field of the  $z = 2.69$  quasar QSO 1213–0017 (UM 485), which is significantly over-abundant compared to the field ERO surface density. The optical/near-IR colors of the EROs and numerous other red galaxies in this field are consistent with elliptical galaxies at  $z = 1 - 2$ . *HST* optical images for a subset of galaxies show regular morphologies,

---

<sup>1</sup>Based in part on observations obtained with the NASA/ESA *Hubble Space Telescope*, which is operated by the STScI for the Association of Universities in Research in Astronomy, Inc., under NASA contract NAS5-26555.

<sup>2</sup>Based in part on observations obtained at the W. M. Keck Observatory, which is operated jointly by the California Institute of Technology and the University of California.

<sup>3</sup>Hubble Fellow

<sup>4</sup>Visiting Astronomer, Kitt Peak National Observatories (KPNO), a division of National Optical Astronomy Observatories, which is operated by Associated Universities for Research in Astronomy, Inc., under cooperative agreement with the National Science Foundation.

most of them being disk-like or diffuse and without any obvious evidence for interactions. Ground-based IR images show similar morphologies, indicating any dust reddening in these objects is spatially uniform. Optical spectroscopy with the W. M. Keck Telescope has found that four of the red galaxies lie at  $z \approx 1.31$ , and a fifth lies in the foreground at  $z = 1.20$ . Of the  $z \approx 1.31$  galaxies, one is a reddened AGN while the remaining three have rest-frame UV absorption-line spectra characteristic of old (few Gyr) stellar populations, similar to the old red galaxy LBDS 53W091 at  $z = 1.55$ . Including the Mg II absorber seen in the QSO spectrum, we find five galaxies at  $z \approx 1.31$  spread over  $1.5 h_{50}^{-1}$  Mpc on the sky. These results suggest we have discovered a coherent structure of old galaxies at high-redshift, possibly associated with a massive galaxy cluster.

*Subject headings:* galaxies: elliptical and lenticular, cD — galaxies: clusters: general — galaxies: evolution — galaxies: stellar content — infrared: galaxies

## 1. Introduction

The observational study of galaxy formation and evolution can broadly be divided into two approaches: (1) searches for primordial galaxies, typically oriented toward high redshifts, in order to scrutinize formation and evolution processes as they occur, and (2) studies of existing old galaxies to decipher their origin and life history from their current properties. With the advent of infrared imaging detectors, a population of infrared-bright, extremely red objects (EROs) have been uncovered which is relevant to both of these approaches.

Elston et al. (1988) discovered a few objects with exceptional optical/IR colors ( $R - K \gtrsim 5$ ) in the first deep near-IR sky survey. While the brightest objects were shown to be  $z \leq 0.8$  ellipticals (Lilly et al. 1988; Elston et al. 1989), their tantalizing conjecture that the fainter ( $K \gtrsim 18$ ) red objects are  $z > 1$  ellipticals has remained unresolved until recently. Subsequent deep infrared imaging of primarily high-redshift radio galaxy and quasar fields serendipitously uncovered handfuls of objects with extreme colors (McCarthy et al. 1992; Eisenhardt & Dickinson 1992; Graham et al. 1994; Hu & Ridgway 1994; Soifer et al. 1994; Dey et al. 1995; Djorgovski et al. 1995). Deep multicolor optical/IR sky surveys have begun to assemble larger samples of these objects using well-defined selection criteria, an essential starting point for statistical studies (Cowie et al. 1994; Hall & Green 1998; Cohen et al. 1999; Barger et al. 1999; McCracken et al. 2000). In particular, the recent availability of  $1024 \times 1024$  pixel IR detectors has made possible surveys for significant numbers of EROs (Thompson et al. 1999).

The use of the designation “extremely red” has varied in the literature. This was especially true in earlier work where the description was applied to any object appearing in IR images but undetected optically. In this paper, we follow Graham & Dey (1996) and use the term “extremely red object” (ERO) for a source with  $R - K > 6$ . This criteria was an operational one, encompassing several IR-detected, optically-invisible sources known at the time, and it has since become widely

used. In particular, Thompson et al. (1999), who have conducted the widest deep  $R - K$  survey to date, also adopt this definition. They confirm EROs defined by this criteria are unusual objects, being the reddest 2% of the  $K \leq 20$  field galaxy population. However, we will also pay attention in this paper to galaxies with  $R - K > 5$ , the criteria used by Elston et al. (1988) and Cohen et al. (1999), as this is about the expected color of passively-evolving elliptical galaxies at  $z \gtrsim 1$ . We will generically refer to this larger sample as “red galaxies.”

EROs are very optically faint ( $R \gtrsim 24$ ) which has hampered studies of these objects. Successful spectroscopy to determine their redshifts and physical nature has only become possible with the development of the Keck 10-m telescope. Recent work has found some members of this “missing population” are luminous ( $\gtrsim L^*$ ) galaxies at  $z > 1$ ; hence determining their origin has direct relevance to the formation of massive galaxies and AGN. Being solely defined by optical/IR color, the few EROs with measured redshifts form a heterogeneous population as expected, comprising at least two broad classes: (1) ultraluminous dusty star-forming systems, perhaps akin to local objects like Arp 220, and (2) massive galaxies with old passively-evolving stellar populations.

The best studied ERO to date, ERO J164502+4626.4 (object 10 of Hu & Ridgway 1994, hereinafter “HR10”), is the prototype for star-forming EROs. This object is a  $z = 1.44$  dusty, ultraluminous galaxy with enormous ongoing star formation ( $\gtrsim 1000 M_\odot \text{ yr}^{-1}$ ) suggested by its sub-mm continuum emission (Graham & Dey 1996; Cimatti et al. 1998; Dey et al. 1999). However, since HR 10 has among the reddest colors ( $I - K = 6$ ) of known EROs, it is unrepresentative of the bulk of the population or at least is an extreme example. These EROs may provide excellent case studies of optically obscured star formation in the early Universe, especially given the association of faint EROs with some of the sub-mm emitting sources found by SCUBA (Smail et al. 1999). In fact, it may be that intense, very brief bursts of star formation are a common mode of star formation at high redshift.

There are also examples of EROs as galaxies with old stellar populations. Passively evolving ellipticals at  $z > 1$  are expected to have large  $R - K$  colors, which stem from their rising spectral energy distributions (SEDs) longward of 4000 Å being redshifted into the near-IR. Therefore, selection using very red colors is an excellent method to search for early-type galaxies at  $z > 1$ . This is especially true in searching for clusters since the surface density of galaxies becomes quite high at faint magnitudes and it would otherwise be hard to distinguish a cluster from the foreground and background populations. However, ellipticals at these distances are expected to be optically very faint so measuring spectroscopic redshifts is challenging. Dickinson (1995) has identified a cluster of elliptical galaxies associated with the powerful radio galaxy 3C 324 at  $z = 1.206$  along with a foreground structure at  $z = 1.15$ . To date, the highest-redshift collection of old, red galaxies spectroscopically confirmed has been found by Stanford et al. (1997). They have discovered a  $z = 1.27$  cluster by its large  $J - K$  colors; the cluster galaxies have  $R - K \gtrsim 5$  and rest-frame UV spectra resembling local elliptical galaxies. There is also a neighboring cluster at  $z = 1.26$  found from its X-ray emission by Rosati et al. (1999) which contains spectroscopically old red galaxies. Isolated examples of old EROs have been discovered at still higher redshifts. The very weak radio

sources LBDS 53W091 at  $z = 1.552$  (Dunlop et al. 1996; Spinrad et al. 1997) and LDBS 53W069 at  $z = 1.432$  (Dunlop 1998; Dey et al. 2000) both have  $R - K \approx 6$  and rest-frame UV spectra which imply ages of a few Gyr. Recently, Soifer et al. (1999) have identified an  $R - K \sim 7$  object as an old galaxy at  $z = 1.58$  based on associating a large continuum break observed at  $\approx 1 \mu\text{m}$  with redshifted 4000 Å break.

Discovery of  $z > 1$  galaxies with old stellar populations offers several powerful lines of inquiry into understanding galaxy formation and evolution and its cosmological context. Detailed comparison of the absorption lines and continuum breaks of these galaxies with galaxies at  $z = 0$  may prove fruitful in tracing the evolutionary course and enrichment history of the oldest stellar populations. Absolute age dating of these galaxies would provide a constraint on the time scale of galaxy formation and the age of the Universe. Moreover, clusters of old galaxies at high redshift can provide testing grounds for competing scenarios of galaxy formation; the predicted appearance of early-type galaxies in these clusters is dramatically different in hierarchical galaxy formation scenarios as compared to monolithic collapse ones (e.g., Kauffmann & Charlot 1998). Finally, the existence of these old galaxies at high redshift potentially can constrain cosmological parameters and theories of structure formation (e.g., Peacock et al. 1998).

We are conducting an on-going study of the nature of these EROs, using deep optical and near-IR imaging from the ground to assemble a large sample of EROs for statistical study. We have been acquiring high-resolution morphological information from *HST* optical and Keck near-IR imaging, and we are obtaining spectroscopy from Keck in the optical and near-IR to determine ERO redshifts and physical properties. Deciphering the identity of EROs based on comparing broadband colors alone to theoretical stellar population synthesis models is dubious given that the model parameter space is vast, at least comprising age, metallicity, and reddening variations. Spectroscopy is essential. In addition, given the apparent heterogeneity of the population, a reasonably large sample of objects needs to be studied to understand the nature and relative abundances of the subsets, instead of the spectroscopy of individual EROs which has been done to date.

In this paper, we present a study of the EROs in the field of QSO 1213–0017 (RA =  $12^h 15^m 49.8^s$ , Dec =  $-00^\circ 34' 34''$ ; J2000.0). This  $z = 2.69$  quasar, also known as UM 485, has exceptionally strong and complex Mg II absorption systems at  $z = 1.3196$  and  $z = 1.5534$  (Steidel & Sargent 1992). In § 2, we describe optical and near-IR imaging covering an  $11 \text{ arcmin}^{-2}$  region around this field and Keck optical spectroscopic follow-up of galaxies selected by their very red colors. We consider in § 3 the surface density of the red galaxies, their morphologies, and their spectroscopic redshifts. We examine in § 4 the collection of red galaxies as a whole, both their spatial distribution to consider the possibility that they are members of a cluster at  $z = 1.31$  and their spectrophotometric properties to understand their stellar populations. We summarize our findings in § 5 and discuss their implications.

Throughout this paper, we assume a cosmology with  $\Omega = 1$ ,  $\Lambda = 0$ , and  $H_0 = 50 h_{50} \text{ km s}^{-1} \text{ Mpc}^{-1}$ . At  $z = 1.31$  with these parameters,  $1'' = 8.58 h_{50}^{-1} \text{ kpc}$ ; the luminosity distance  $d_L = 9.40 h_{50}^{-1} \text{ Gpc}$ ;

and the angular diameter distance  $d_\theta = 1.78 h_{50}^{-1}$  Gpc.

## 2. Observations

### 2.1. Optical Imaging

Optical imaging of the field of QSO 1213–0017 was obtained in April 1993 using the KPNO 4-m Mayall telescope as part of a program to image  $z > 1$  Mg II absorbing galaxies near QSO sightlines (see Steidel 1995). We used the PFCCD equipped with a  $2048 \times 2048$  Tektronix CCD and a pixel scale of  $0''.47/\text{pixel}$ . A total integration of 3500 s was obtained through the  $\mathcal{R}$ -band filter ( $\lambda_c = 6930 \text{ \AA}$ ,  $\Delta\lambda = 1500 \text{ \AA}$ ) under photometric conditions and  $1''.25$  FWHM seeing. The data were reduced using standard techniques and calibrated onto the AB magnitude system<sup>5</sup> using spectrophotometric standard stars from the lists of Massey et al. (1988) and Oke & Gunn (1983). The  $\mathcal{R}$  filter is a compromise between the standard Cousins  $R_C$  and  $I_C$  filters. A filter trace for  $\mathcal{R}$  and a photometric transformation to the Kron-Cousins system are given in Steidel & Hamilton (1993). For the very red objects considered in this paper,  $\mathcal{R} \approx R_C$  after accounting for the color terms, so the  $\mathcal{R} - K$  colors given for the EROs in this paper are roughly equivalent to  $R_C - K$  colors given for other EROs in the literature (see § 3.1).

We obtained four images of the 1213–0017 field with the WFPC2 camera aboard *Hubble Space Telescope (HST)* on U.T. 1998 January 11. Data were taken using the  $F814W$  filter with a total integration of 4500 s. The integrations were taken in slightly offset positions, allowing reasonable identification of cosmic ray hits in the individual images which were then excluded from the averaging to create the final image.

### 2.2. Near-IR Imaging

#### 2.2.1. KPNO

Infrared data were obtained in February 1994 on the KPNO 4m Mayall telescope using the IRIM imager, equipped with a  $256 \times 256$  NICMOS-3 HgCdTe detector and sampling the sky at  $0''.60/\text{pixel}$ . A total integration time of 3660 s was obtained in a non-repetitive grid, in which the telescope was moved after each 60 s of integration time. Conditions were photometric with  $1''.0$  FWHM seeing. The data were reduced using the DIMSUM package (Eisenhardt, Stanford,

---

<sup>5</sup>Note that our preliminary results in Liu et al. (1999) designated the  $\mathcal{R}$  filter as “ $R_S$ ” and presented Vega-based magnitudes, instead of AB ones. For the  $\mathcal{R}$  filter, the offset from AB mags to Vega-based mags is  $-0.28$  mag, i.e.,  $\mathcal{R}^{Vega} = \mathcal{R}^{AB} - 0.28$ .

Dickinson, & Ford, priv. communication) in IRAF.<sup>6</sup> The data were calibrated using the UKIRT faint standards (Casali & Hawarden 1992), resulting in Vega-based magnitudes. The data were taken in the  $K_S$  filter (McLeod et al. 1995) which is slightly bluer and narrower than the standard  $K$  filter. As discussed by Hall et al. (1998), the shift between  $K_S$  and  $K_{UKIRT}$  is expected to be quite small, less than 0.04 mag for objects as red as  $H - K = 1$ . In the absence of IR colors for all the objects to compute color terms, we assume  $K_S = K$  hereinafter, which will have a negligible effect on any of our results.

### 2.2.2. Keck

We obtained deeper, higher spatial resolution IR imaging of two sub-fields on U.T. 1998 May 14–15 using the facility near-IR camera NIRC (Matthews & Soifer 1994) of the 10-meter W. M. Keck I Telescope located on Mauna Kea, Hawaii. The camera employs a Santa Barbara Research Corporation  $256 \times 256$  InSb array and has a pixel scale of  $0''.150$ /pixel resulting in a  $38''$  field. We observed 2 fields close to the quasar, one to the southwest (containing R4, R5, and R6) and one to the northeast (containing R7, R9, and R10). The SW field, centered about  $(-27''$  E,  $-7''$  N) from QSO 1213–0017, was observed with the standard  $JHK$  filters with integration times of 900, 2040, and 2280 s, respectively, totaled over the two nights. The NE field, centered about  $(27''$  E,  $10''$  N) from QSO 1213–0017, was observed in  $J$  for 780 s and in  $K$  for 1200 s on 15 May 1998 UT. We used integration times of 6 or 20 s per coadd, depending on the filter. After one minute of integration was coadded, the sum was saved as an image, and then the telescope was offset by a few arcseconds. The telescope was stepped through a non-redundant dither pattern, and an off-axis CCD camera was used to guide the telescope during the observations. Conditions were non-photometric while observing the NE field and also for part of the SW field observations. For the SW field, we culled frames which were non-photometric from the reduction process. For the NE field, the data are used only to examine morphologies.

The data were reduced in a manner typical for near-IR images. An average dark frame was subtracted from each image to remove the bias level. We constructed a flat field by median averaging scaled images of the twilight sky. A preliminary sky subtraction of the images was performed to identify astronomical objects. Then for each image, we subtracted a local sky frame constructed from the average of prior and subsequent images, excluding any of the identified astronomical objects from the averaging. We used the brightest source in each field to register the reduced frames, which were then shifted by integer pixel offsets and averaged to assemble a mosaic of the field. Bad pixels were identified by intercomparing the registered individual images and masked during the construction of the mosaic. All these reductions were done using custom software written for Research System Incorporated’s IDL software package (version 5.1).

---

<sup>6</sup>IRAF is distributed by the National Optical Astronomy Observatories, which are operated by the Association of Universities for Research in Astronomy, Inc., under cooperative agreement with the National Science Foundation.

We observed the faint HST IR standard SJ 9143 (Persson et al. 1998) as a flux calibrator so the resulting magnitudes are Vega-based. Aperture photometry of the registration object in each individual frame verified the SW field data which were retained were nearly photometric, with any systematic errors of order 5% or less. There are no obvious point sources in the images, but the most compact objects have a FWHM of  $\approx 0''.5$ .

### 2.3. Optical/Near-IR Photometry

To identify very red objects, we compiled a photometric catalog of all objects in the KPNO  $K$ -band mosaic using the SExtractor software of Bertin & Arnouts (1996), version 2.0.21. Each pixel in the  $K$ -band image was multiplied by the square root of its exposure time to create a mosaic with uniform noise over the entire field. Objects in the noise-normalized mosaic were then identified as any set of contiguous pixels  $1.5\sigma$  above the background level with an area equal to a FWHM-diameter circular aperture (10 pixels), i.e., a highly significant detection, and then aperture photometry was done on the original  $K$ -band image. We used the resulting “MAG\_BEST” magnitudes, which for uncrowded objects use apertures determined from the moments of each object’s light distribution. This method is similar to that of Kron (1980) and is designed to recover most of an object’s flux while keeping errors low. The  $\mathcal{R}$  image was transformed to be registered with the  $K$  image, and photometry was done using the same apertures for each object as for the  $K$ -band image. The Galactic reddening towards this field is small,  $E(B-V) = 0.02$  (Schlegel et al. 1998), so we apply no extinction corrections to the photometry.

We ran Monte Carlo simulations to verify the accuracy of the measured magnitudes and errors. We inserted 10 artificial stars of known magnitude and color into the images and then processed the images with SExtractor in the same fashion as the original data. For each magnitude and color bin, we ran the simulation 30 times for a total of 300 stars and then compared the recovered magnitudes and colors to the input ones in order to determine the random and systematic photometric errors. The artificial stars were chosen to span a range in magnitude and color encompassing all the real objects, with 0.5 mag steps in  $K$  magnitude and 1 mag steps in  $\mathcal{R}-K$  color. A low-order polynomial surface was then fitted to the photometric errors from the simulations as a function of  $K$  magnitude and  $\mathcal{R}-K$  color, and the fit coefficients were used to assign photometric errors for the real objects. In all cases the systematic offset from the input magnitude to mean recovered magnitude for the artificial stars was always much smaller than the  $1\sigma$  random errors, so we applied no systematic corrections to the photometry of the real objects. The errors produced by SExtractor were found to agree well with the errors deduced from the simulations, except for objects near the detection limit. In principal, there will be a surface brightness dependence since errors measured from stars will not be the same as those measured from less compact sources such as galaxies (e.g., Bershady et al. 1998). However, this effect is more important for determining the completeness corrections, which is not relevant to our work here, and, furthermore, at the faint limit the majority of our sources are nearly unresolved so any error in measuring the error will be negligible.

Since the Keck/NIRC imaging reaches fainter magnitudes than the KPNO data, they were processed separately, but using SExtractor in an analogous fashion. Objects were identified and photometric apertures were determined from the  $K$ -band image. This information was used to process the other bands, with Monte Carlo simulations used to compute photometric errors.

#### 2.4. Optical Spectroscopy

We observed the 1213–0017 field with the 10-m Keck II Telescope using the facility optical spectrograph LRIS (Oke et al. 1995) on U.T. 1999 June 15. We prepared a focal plane mask of 1''.5-wide slitlets to observe seven objects with  $\mathcal{R} - K > 5$ . The length of each slitlet varied, with a minimum length of 14''. We used the 150 lines/mm grating blazed at 7500 Å to cover a nominal wavelength region from 4000–10000 Å, depending on the position of the slitlets on the mask. The dispersion of  $\approx 4.8$  Å/pixel resulted in a spectral resolution of  $\approx 25$  Å, as measured by the FWHM of a few strong emission lines of serendipitous objects and the lines of the calibration arc lamp spectra. Sky conditions were photometric with seeing of 0''.45 at the start of the integrations. We obtained 3 exposures of 1800 s each with the mask oriented at a position angle of 46° east of north. We dithered the telescope a few arcseconds along the slit direction between each exposure.

The slitmask data for the objects were separated into seven individual spectra and then reduced using standard longslit tasks in IRAF. The data were bias-corrected using the unilluminated pre- and post-scan regions of the detector and flat-fielded using internal quartz lamps obtained immediately after the observations. Sky lines were subtracted by fitting a low-order analytic function to each column of the images, perpendicular to the dispersion axis. We corrected each exposure for long-wavelength fringing by taking an average of the other 2 exposures and subtracting this average. The exposures were registered and combined. The most compact objects in the resulting mosaic are  $\approx 0''.6$  FWHM in the spatial direction, though they may not be point sources. A 1-d spectrum of each red galaxy was extracted using a 1''.3 (6 pixel) wide aperture and was wavelength-calibrated using HgKr and NeAr lamps taken immediately after the observations, with an RMS of  $\approx 0.3 - 0.4$  Å in the wavelength solutions. Zeropoint shifts of  $\leq 2$  Å were applied to the spectra based on the measured wavelengths of the night sky lines. Flux calibration was performed using the standard star G191B2B (Massey et al. 1988; Massey & Gronwall 1990)

### 3. Results

#### 3.1. An Excess of EROs

Figure 1 presents the KPNO  $\mathcal{R}$ -band and  $K$ -band images of the 1213–0017 field, which cover an area of  $11.2 \text{ arcmin}^{-2}$ . Figure 2 shows the field’s color-magnitude diagram along with the no-evolution locus of local elliptical galaxies redshifted to  $z = 1.3$ , computed from multicolor

photometry of the Coma cluster as described in Stanford et al. (1998). If we were to account for passive stellar evolution, the locus would appear somewhat bluer and brighter.

A population of objects with red ( $\mathcal{R} - K > 5$ ) colors are found starting at  $K \approx 18$  mag, irregularly distributed on the sky. Most of the galaxies are somewhat bluer than the Coma locus at  $z = 1.3$ , and the brightest of the EROs have  $K$ -band fluxes comparable to the brightest Coma cD galaxies. As we discuss below, there is a significant excess of red objects in this field compared to the surface density measured from blank sky surveys. However, before analyzing the counts of the reddest objects, we must first account for a few issues: (1) the effective wavelength of the  $\mathcal{R}$  filter is significantly redder ( $\approx 350$  Å) than the standard Cousins  $R_C$  filter; (2) our data becomes incomplete at  $K \gtrsim 19.5$ , as gauged by the turnover in the number counts; and (3) the exposure time is not uniform over the field, with only about half the field receiving at least 50% of the maximum integration. (Also, there will be some added uncertainty since the abundance of the reddest objects has a strong dependence on the choice of color and magnitude cuts.)

The most extensive  $R - K$  color-selected counts in a blank field of the sky come from the CADIS survey of Thompson et al. (1999). They find a surface density of  $0.039 \pm 0.016 \text{ arcmin}^{-2}$  in an area of  $154 \text{ arcmin}^2$  for the bright EROs ( $R - K' > 6$  and  $K' < 19$ ), slightly revised to  $0.047 \pm 0.009 \text{ arcmin}^{-2}$  in their final survey area of  $600 \text{ arcmin}^2$  (D. Thompson, priv. communication). Direct comparison of our ERO counts with theirs is complicated as their  $R_{CADIS}$  filter is  $\approx 450$  Å bluer than our  $\mathcal{R}$  filter. Because EROs are very red and their number counts are a strong function of  $R - K$  color, the difference is significant. (The difference in IR filters, their  $K'$  versus our  $K_S$ , is much less important.) We computed the offset between  $R$  filters as a function of redshift using the elliptical galaxy SED of Coleman et al. (1980). The true SEDs of the ERO population(s) are unknown, but we adopt this template as a reasonable guess. At  $z = 0$ ,  $(R_{CADIS} - \mathcal{R})$  is  $-0.08$  mag; the difference is negative due to the fact that  $\mathcal{R}$  mags are AB and  $R_{CADIS}$  mags are Vega-based (see footnote 5). This difference increases nearly monotonically with redshift out to  $z \approx 1.5$ , becoming as large as 0.4 mag. For redshifts of  $0.5 - 1.7$ , the calculated offset is  $\geq 0.17$  mag. Since the few EROs with known redshifts lie in this range, we add 0.17 mag to our measured  $\mathcal{R} - K$  colors to compare to the Thompson et al. results. This is the minimum expected amount for the transformation (i.e., an ERO at  $z = 0.5$ ) and therefore leads to conservative estimates for the 1213–0017 ERO overdensity.

After accounting for this difference in filters, we find five  $K \leq 19$  objects with  $(R_{CADIS} - K) > 6$  in our images, four of which lie in the central  $6.2 \text{ arcmin}^2$  area which received least half of the maximum integration time. Since the counts over the whole mosaic are guaranteed to be incomplete, we consider only this central region. The counts of Thompson et al. (1999) predict 0.24 objects in a  $6.2 \text{ arcmin}^2$  area,  $16 \times$  fewer than observed. The Poisson probability of our observing four or more EROs given the expected surface density is only  $1.1 \times 10^{-4}$ , i.e., the overabundance of EROs in the 1213–0017 field is highly statistically significant. The probability grows to 5% if the blank sky counts are increased by a factor of 5.7, i.e., the 1213–0017 ERO surface density is overabundant by this factor at the 95% confidence level.

Similarly, with the less restrictive color criteria of  $(R_{CADIS} - K) = 5 - 6$ , where the blue cutoff is about the color of a passively evolving single-burst population at  $z \gtrsim 1$  (Figure 9), the Thompson et al. (1999) data predict 2.4 objects with  $K \leq 19$  while we observe 7 objects. The Poisson probability of finding at least this many objects is  $1.2 \times 10^{-3}$ , and the enhancement of such objects in the 1213–0017 field is at least a factor of 1.4 at the 95% confidence level.

We can combine the counts in the  $(R_{CADIS} - K) > 6$  and  $(R_{CADIS} - K) = 5 - 6$  bins to compute the enhancement of the 1213–0017 field over the blank sky counts. We compute the joint probability of observing the 4 and 7 galaxies in these two color bins over a range of enhancement factors and find the most likely excess is a factor of 4.2, with the 95% confidence range being factors of 2.2–7.1. Note that this calculation assumes the enhancement is the same for both color bins, which may not be the case.

### 3.2. Morphologies of the Red Galaxies

Figure 3 and 4 show the reduced Keck/NIRC  $K$ -band mosaics for the fields NE and SW of QSO 1213–0017. Note that the images reach different limiting depths; the faintest objects in the NE and SW data are  $\approx 20.5$  and  $21.3$  mag, respectively. We compare these data with the *HST*  $F814W$  images in Figure 5 to examine the observed optical and IR morphologies of the objects with  $\mathcal{R} - K > 5$ . The *HST* images are centered on the QSO so we do not have images for the red galaxies farther away, including unfortunately R1 and R8 for which we have continuum-break spectroscopic redshifts (§ 3.3.2). For  $z = 1.3$ , these datasets roughly correspond to the rest-frame near-UV/blue ( $3100 - 4100$  Å) and far-red ( $8700 - 10400$  Å). [O II]  $\lambda 3727$  emission lies in the  $F814W$  filter bandpass for objects at  $z \approx 0.9 - 1.5$ . All the red objects are extended in the *HST* images meaning they cannot be galactic M dwarfs. A few of them appear to be E/S0 type. The *HST* images are relatively shallow ( $3\sigma$  limiting surface brightness  $\mu_{F814W} \approx 25.7$  mag arcsec $^{-2}$ ), but we can still see faint emission around a number of the red galaxies. Several seem to have both a central spheroid and a faint component suggestive of a disk, while a few are entirely diffuse emission without any compact core/bulge. None show any strong evidence for interactions. Overall, the detected red galaxies show remarkable consistency in their morphologies between the  $F814W$  and  $K$ -band images. We return to this issue in § 4.2.1.

### 3.3. Optical Spectroscopy

From the 2-d reduced spectra, we were able to identify spectroscopic features in five of the red galaxies on our slitmask, both from emission lines and continuum breaks (Table 1). To more accurately determine the redshifts and their errors, we used the Fourier cross-correlation technique of Tonry & Davis (1979) as implemented in the FXCOR task of IRAF. We linearly interpolated over significant residuals in the spectra resulting from imperfect cancellation of the strongest telluric

features. The three absorption-break galaxies were cross-correlated against the UV spectra of F and G dwarfs from the *IUE* Spectra Atlas of Wu et al. (1991), using an average spectrum for each spectral type. The spectra of the emission-line galaxies were cross-correlated against the emission-line template of an Sc galaxy from Kinney et al. (1996).

### 3.3.1. *R6 and R7 — Emission-Line Galaxies*

The spectrum of R6 shows a single emission line with an observed equivalent width (EW) of  $\approx 60$  Å (Figure 6). There is ample continuum blueward of the line so we identify it as [O II]  $\lambda 3727$ , placing R6 at  $z = 1.203$ , slightly in the foreground of the other redshifts in this field. Assuming this emission originates from H II regions of massive young stars, we infer a star formation rate of  $\approx 10 h_{50}^2 M_{\odot} \text{ yr}^{-1}$  using the [O II] calibration of Kennicutt (1992), comparable to the most active spirals in the local neighborhood (Kennicutt 1983).

The spectrum of R7 reveals the presence of an active galactic nucleus at  $z = 1.319$  (Figure 6). The data show strong lines of [O II]  $\lambda 3727$  and C II]  $\lambda 2326$  with observed equivalent widths of  $\approx 50$  Å. The C III]  $\lambda 1909$  line is possibly detected, though this line falls near the blue end of the spectrum where the signal is quite low. Examination of the reduced images clearly shows a weak [Ne IV]  $\lambda 2424$  emission line which lies on the red edge of the strong [O I]  $\lambda 6300$  telluric line, preventing a good measurement. Strangely, no Mg II  $\lambda 2800$  emission line is seen, even though it is typically at least as strong as [Ne IV]  $\lambda 2424$  and C II]  $\lambda 2326$  in high- $z$  AGN (e.g., Stern et al. 1999). Presumably the emission line is absorbed by gas in this galaxy though no strong Mg II  $\lambda 2800$  absorption feature is seen. Also, there are some possible weak absorption features in the 8800–9200 Å range near the expected location of the higher order Balmer lines, in particular at 8896 Å which matches the Balmer H9 transition. However, spectra become quite noisy in this region and the features are not overly compelling. Finally, there are no signs of an old stellar population as the strongest continuum breaks (B2640, B2900, D4000) and the Ca H+K lines are all absent.

### 3.3.2. *R1, R8, and R10 — Old Continuum-Break Galaxies*

Three of the red galaxies on our slitmask — R1, R8, and R10 — are devoid of strong emission lines (Figures 7), but they do show continuum breaks identifiable as the rest-frame mid-UV (2000 – 3300 Å) breaks of B2640 and B2900 at  $z = 1.317$ , 1.298, and 1.290, respectively. The breaks arise from metal-line blanketing on either side of the tophat-shaped feature from 2640–2720 Å. These features, which were first suggested by Morton et al. (1977) as possibly being useful for redshift determinations at  $z > 0.75$ , have been used recently to identify old galaxies out to  $z \approx 1.55$  (Dunlop et al. 1996; Dey et al. 2000). At least two of the red galaxies may also have Mg II  $\lambda 2800$  in absorption. These spectral features are characteristic of old stellar populations, such as Galactic and M31 globular clusters, M32, and the cores of local elliptical galaxies (e.g., Rose & Deng 1999;

Ponder et al. 1998, and references therein). Galaxies R8 and R10 also may show the 4000 Å break at  $\approx 9200$  Å.

For these three galaxies, we determined the redshifts using the 4300–8000 Å region of the spectra in the cross-correlation analysis. At longer wavelengths, the random errors increase from enhanced telluric OH emission, and the systematic errors also increase from imperfect removal of the CCD fringing pattern, due to the small number of exposures we were able to acquire. In addition to the choice of wavelength region, another important aspect of the redshift determination is the choice of stellar template. We explored template spectra ranging from spectral types F0 to G8, using both the Fourier analysis and a direct computation of the cross-correlation between galaxy and template as a function of redshift. All templates produced fairly consistent redshifts using both methods. Figure 8 shows the rest-frame galaxy spectra with *IUE* stellar spectra overplotted for comparison.

## 4. Discussion

### 4.1. A Concentration of Red Galaxies at $z = 1.31$

We have measured five redshifts for the red galaxies in the 1213–0017 field. Four of these lie near  $z = 1.31$  with the remaining one at  $z = 1.203$ . The spectrum of QSO 1213–0017 also shows an Mg II absorption system at  $z = 1.3196$  (Lanzetta et al. 1987; Steidel & Sargent 1992), similar to the redshift of  $1.319 \pm 0.002$  for galaxy R7. Could this galaxy be responsible for the absorption? It is located  $15''$  from the QSO, which is  $130 h_{50}^{-1}$  kpc. Based on preliminary results from a survey of  $z = 0.3 - 0.9$  Mg II absorbers by Steidel (1993) and Steidel & Dickinson (1995), the median projected impact parameter between QSOs and their best candidate absorber is  $45 h_{50}^{-1}$  kpc with an upper bound of  $80 h_{50}^{-1}$  kpc. Early results from their  $z > 1$  survey find the absorber properties are not dramatically different compared to the lower redshift sample (Steidel 1995; Dickinson & Steidel 1996). The projected separation of R7 therefore seems too large for it to be the Mg II absorber, though the geometry and extent of Mg II absorption systems remain open questions (c.f. Steidel 1995; Charlton & Churchill 1996). In addition, our *HST* images show a few faint galaxies with projected separations from the QSO of  $\lesssim 80 h_{50}^{-1}$  kpc, making them better candidates for the absorber. Since R7 is unlikely to be the Mg II absorber, we infer that there is at least one more galaxy at  $z = 1.3196$ .

Including the Mg II absorber, there are five galaxies within an angular region of  $3'$  and close together in velocity. Their redshifts have an unweighted mean of 1.309 and a standard deviation  $\sigma = 1790 \pm 570$  km s $^{-1}$  in the mean rest frame.<sup>7</sup> The full spread in redshift is 3800 km s $^{-1}$  in

<sup>7</sup>The above results use the standard formulae. Similar results are obtained using the central location (“mean”) and scale (“dispersion”) estimators recommended by Beers et al. (1990) for non-Gaussian velocity distributions. Their preferred central location measures for a sample of this size, the median and the biweight-estimated mean, give

the mean rest frame; for comparison, consider that 95% of the galaxies in the central  $6 h_{50}^{-1}$  Mpc of the Coma cluster and with  $cz < 12,000$  kms lie within  $\pm 3500$  km s $^{-1}$  (Postman et al. 1998). The considerable dispersion and range of the 1213–0017 redshifts are possibly due to velocity sub-structure in this field. There is a hint of this in the data: two of the galaxies (R8 and R10) lie at  $z = 1.290 - 1.298$  while the other three are at  $z = 1.317 - 1.320$ , i.e., there is a “gap” of 2500 km s $^{-1}$  in the mean rest frame, although there is no clear segregation of the two subsets on the sky. We may be seeing two separate physical entities close in redshift (e.g., filaments/sheets/sub-clusters) which may later merge into one, but this speculation lies beyond the available data.

Interestingly, the few known  $z \approx 1$  massive clusters show large velocity dispersions and/or signs of sub-structure, e.g., the 3C 324 “cluster” at  $z = 1.15$  and  $1.21$  (Dickinson 1997); RX J1716.6+6708 at  $z = 0.81$  (Henry et al. 1997; Gioia et al. 1999; Clowe et al. 1998); and CL 0023+0423 at  $z = 0.84$  (Postman et al. 1998; Lubin et al. 1998). Spectroscopically confirmed galaxies in these clusters have angular extents of a few arcminutes but are not strongly concentrated on the sky, which is also the case for the red galaxies in the 1213–0017 field. In the case of ClG J0848+4453 at  $z = 1.27$  and the neighboring RXJ0848.9+4452 at  $z = 1.26$  (Stanford et al. 1997; Rosati et al. 1999), each individual cluster is fairly compact but taken together these two add up to an entity with a large velocity range separated by only a few arcminutes.

In addition to the galaxies with spectroscopic redshifts, we can use optical/IR colors to constrain the redshifts of objects in the SW field, the only one with photometric data in all filters (see § 2). The galaxies’  $\mathcal{R}JK$  colors are consistent with Bruzual & Charlot (1996) models of old stellar populations at  $z = 1 - 2$  (Figure 9), with the identification largely based on the change in  $\mathcal{R} - J$  color. The  $JHK$  colors provide less sensitivity, but they are consistent with the same redshift interval (Figure 10).

To summarize, the collection of red galaxies in the 1213–0017 field is concentrated in redshift at  $z \approx 1.31$ . The small number of measured redshifts prevents any definitive conclusions, but the redshifts do have a considerable spread. The red galaxies are spread over  $\approx 1.5 h_{50}^{-1}$  Mpc on the sky, with a surface density about a factor of four above  $R - K > 5$  counts and a factor of 16 above bright ERO counts in blank fields (§ 3.1). Although we do not know all their redshifts, it is quite plausible that most of the red galaxies are at  $z = 1.31$ , as we discuss in the next section.

## 4.2. Old Stellar Populations at $z = 1.31$

### 4.2.1. Origin of the Extremely Red Galaxy Colors

With the Keck and *HST* findings, we now examine more closely the origin of the colors of the 1213–0017 red galaxies and EROs. Their colors are consistent with  $z > 1$  ellipticals (Figures 2

---

$z = 1.317$  and  $1.319$ , respectively. The gapper method they advocate for computing the scale gives 1840 km s $^{-1}$ .

and 9), and we have confirmed this inference for three of them using Keck spectroscopy. For these galaxies there is little doubt the large  $\mathcal{R} - K$  colors are due to old stellar populations with a negligible amount of dust. For the red galaxies in the SW field, their  $\mathcal{R}JHK$  colors are also consistent with unreddened  $z = 1 - 2$  ellipticals (Figures 9 and 10); the one SW galaxy with a Keck spectrum, R6, supports this idea as it lies at  $z = 1.203$ , though its redshift is based on weak [O II] emission. (The spectrum has insufficient S/N to detect any continuum breaks, if present.) So even if R6 is composed of an old, red stellar population (its  $\mathcal{R}$ -band flux is only marginally brightened by the [O II] line), the emission line points to a small amount of simultaneous star-formation or weak AGN activity. In fact, R6 has quite a different appearance in optical as compared to the near-IR (Figure 5) which may suggest significant dust reddening in its central regions, unlike most of the other red galaxies (see below).

The other galaxy with a spectroscopic redshift, R7, has an optically revealed AGN. Its  $\mathcal{R} - K$  color is far too red compared to typical Seyferts (e.g., Kotilainen & Ward 1994). Its redness might come from dust or from old stars, although its optical spectrum shows no signs of the latter. If the Balmer features in the spectrum are real, this would suggest R7 has experienced significant star formation in the last few  $\sim 10^8$  years and would hint that the red colors are due to dust reddening.

For the remaining 1213–0017 red galaxies, we have no direct evidence about their redshift nor their stellar content; all that we know is their  $\mathcal{R} - K$  colors. One unlikely cause for their redness would be a strong emission line redshifted into the  $K$ -band; the lowest possible redshift for this to occur would be for  $\text{H}\alpha$  at  $z \approx 2.1 - 2.6$ . It seems implausible that all or even any of these galaxies are at this redshift given the very low surface density of strong high-redshift  $\text{H}\alpha$  emitters (e.g., Thompson et al. 1996; Beckwith et al. 1998; Teplitz et al. 1998). In fact, the more likely case of emission-line contamination of the broad-band magnitudes is in the  $\mathcal{R}$ -band, either from  $\text{H}\alpha$  or [O II]; more than half of  $z = 0.5 - 1.3$  field galaxies show [O II] emission (Hammer et al. 1997). In this case, the measured  $\mathcal{R} - K$  colors would be slightly bluer than the true color of the underlying stellar continuum.

We find the observed optical and near-IR morphologies are fairly regular and in good agreement with one another (Figure 5). Both of these tell us that dust reddening in these galaxies is spatially uniform on scales of  $\lesssim 4 h_{50}^{-1}$  kpc, as small as  $\approx 0.9 h_{50}^{-1}$  kpc for the *HST* images. This is in sharp contrast to the highly wavelength-dependent appearance of the prototypical ERO HR 10: in the rest-frame near-UV/blue it has an inverted S-shape while in the rest-frame red it shows a smooth compact appearance (Dey et al. 1999). This implies HR 10 is an interacting/disturbed system whose central region has a large amount of dust, an interpretation augmented by its sub-mm emission which presumably springs from a large amount of ongoing dusty star formation. *HST* optical morphologies for the first sub-mm selected sources, which are possibly similar to HR 10, also show disturbed appearances (Smail et al. 1998). Likewise, the rest-frame UV appearance of local ultraluminous *IRAS* galaxies (ULIRGs) are significantly different than their appearance at longer wavelengths (Trentham et al. 1999).

Therefore, we conclude the wavelength-independent appearance of the 1213–0017 red galaxies means they are unlikely to be dusty star-forming galaxies like HR10 or ULIRGs. Though dust reddening may still play a role, most of their redness probably originates from the light of old stars. Dust variations could still exist on spatial scales below our resolution limits. For this reason, attempts to fit the broad-band SEDs are potentially misleading given the uncertainties in the dust geometry and distribution — such fits would be highly degenerate. Near-IR images with comparable spatial resolution to the *HST* optical data are needed to address this possibility.

#### 4.2.2. Rest-Frame UV Spectral Features

Comparisons between the galaxy spectra and the *IUE* stellar spectra show the three continuum-break galaxies have real differences in their rest-frame mid-UV spectra. The spectra of R10 rises most rapidly to the red and has the strongest 2640 Å and 2900 Å breaks, while R1’s continuum is noticeably flatter and its breaks are the weakest, especially the 2900 Å break. R8’s spectrum is intermediate between R10 and R1. Results from both cross correlation analysis (§ 3.3.2) and examination by eye find R1 is best-matched by early-type F dwarfs, R8 by mid-type F dwarfs, and R10 by late-type F and early-type G dwarfs (Figure 8) in this wavelength region. Furthermore, even when the *IUE* spectra are normalized only to the galaxy flux longward of 3000 Å, there is still good agreement between the star and galaxy spectra all the way to the bluest wavelengths. This suggests any ongoing or recent star formation, which would be revealed by a rising blue continuum, is small.

The UV continuum breaks at 2640 Å and 2900 Å are of special interest. This region of an old galaxy’s SED is expected to be dominated by light from stars near the main-sequence turnoff. As the stellar population ages, the main-sequence turnoff mass decreases, and later-type stars produce the UV SED, leading to larger break amplitudes. In this fashion the rest-frame UV spectrum might be used to age date the stellar population, or at least the portion contributing the bulk of the UV flux. Spinrad et al. (1997) attempted to do this in a robust fashion for the old galaxy LBDS 53W091 at  $z = 1.55$ . Given difficulties of absolute age calibration for these features and their uncertain metallicity dependence (Heap et al. 1998; Yi et al. 1999a), we do not attempt to age date the populations of the 1213–0017 galaxies.

However, we can still study the stellar content of the spectroscopically old 1213–0017 galaxies by comparing the strength of these breaks with old populations in the local Universe. The spectra of R8 and R10 are barely amenable to this line of investigation, but the S/N of R1’s spectrum is too low so we exclude it. The standard indices for measuring these breaks, 2609/2660 and 2828/2921 from Fanelli et al. (1990), are too narrow for our spectra: these use  $\approx 25$  Å wide bandpasses, meaning they include only 2–3 spectral resolution elements for our data. Instead, we use our own broader custom indices, W2640 and W2900. We also measure the moderate-bandwidth 2600 – 3000 index of Fanelli et al. (1990) to track the UV continuum color. These are all calculated in the standard

fashion, from the ratio of the fluxes in blue and red bandpasses and expressed in magnitudes:

$$\text{Index} \equiv -2.5 \times \log_{10} \left[ \frac{\bar{F}_\lambda(\text{blue})}{\bar{F}_\lambda(\text{red})} \right], \quad (1)$$

where  $\bar{F}_\lambda$  is the average flux density in the bandpasses. Objects with stronger breaks have larger values for the indices. The red bandpass of W2640 covers the entire top-hat feature redward of the 2640 Å break and ends before the Fe+Cr absorption at 2745 Å; the blue bandpass has the same width and includes Fe II λ2609 absorption and part of the broad BL λ2538 feature (e.g., see Ponder et al. 1998). The blue bandpass of W2900 spans the Mg II λ2800 and Mg I λ2852 absorption, and the red bandpass is chosen to have the same width. Definitions and measurements of the standard indices and our custom ones are listed in Table 2.

Figure 11 plots the results juxtaposed against individual main-sequence stars (Fanelli et al. 1992), local old spheroids (Ponder et al. 1998), and the  $z = 1.552$  galaxy LBDS 53W091. The UV indices of R8 and R10 are consistent with local populations, though the W2640 strengths of R8 and R10 differ, with the former having a weaker 2640 Å break than even the local elliptical sample. Also, the two galaxies have different 2600 – 3000 colors, with R8 lying closer to the metal-poor local populations, which have bluer mid-UV colors. The similar break amplitudes of LBDS 53W091 and R10 suggest these two galaxies are comparably old. If the analysis of 53W091’s spectrum is correct, its inferred age is barely compatible with present cosmological parameters, even with the assumption of solar metallicity to reduce the inferred age (Spinrad et al. 1997). Therefore, R10 must have had a comparably high formation redshift, since the difference in look-back time is only 5% between  $z = 1.55$  and  $z = 1.31$ , and also must have experienced little or no recent star-formation.

For the local populations, the offset of the ellipticals from the stars and globular clusters in plots of the 2640 Å break versus 2600–3000 color was noticed by Ponder et al. (1998), who suggested it was due to the hot UV-excess (UVX) population in elliptical galaxies. The UVX is thought to originate from post-main sequence stars, though its specific origin remains uncertain (O’Connell 1999). Interestingly, galaxy R8 does appear to be more consistent with the local ellipticals than the local non-UVX populations which might suggest a hot component in R8. If this could be confirmed for this galaxy and other high-redshift ellipticals, a detailed study of their UV spectra might uncover the origin of the UVX emission, since the potential UVX candidates evolve on different time scales (e.g., Brown et al. 1998; Yi et al. 1999b). However, ongoing star formation, even just a small amount by mass, can greatly brighten a galaxy’s UV flux, thereby complicating such an analysis.

To summarize, comparison of the rest-frame UV spectra of R1, R8, and R10 shows a real scatter in their stellar content even though their observed  $K$ -band fluxes, which should roughly trace galaxy mass, are within a factor of two of each other. This may reflect differences in their star formation and/or merging histories. The UV color and break amplitudes of R8 and R10 are consistent with  $z = 0$  old stellar populations, though the data’s limited S/N and spectral resolution hinders any more detailed comparison, e.g., studying the weaker Mg II and Mg I absorption features. At a redshift of 1.3, we are observing these old galaxies when the Universe was only 30% of its present

age. Therefore, improved data, both in S/N and spectral resolution, could probe the evolving composition of the oldest stellar populations from their relative youth at high redshift to their advanced age at  $z = 0$ .

#### 4.2.3. Relation to Galaxy Morphology and Implications for Formation

The morphological results from the *HST* images are somewhat surprising if our suggestion that the 1213–0017 red galaxies contain old stars is correct. Most of the galaxies do not seem to be early-type ones but rather are disk or diffuse. Indeed, the one absorption-break galaxy with *HST* imaging, R10, looks like a compact edge-on disk — this galaxy does not resemble an elliptical galaxy morphologically even though it does so spectroscopically. These findings argue that not all old EROs are necessarily ellipticals, at least in their structure. This may reflect a fundamental ambiguity in identifying ellipticals at  $z > 1$  as compared to those at  $z = 0$ : are elliptical galaxies properly defined by their morphological or spectrophotometric properties (c.f. Kauffmann et al. 1996; Schade et al. 1999)? If they formed by monolithic collapse at very high redshift, there should be no ambiguity. But in current scenarios of hierarchical galaxy formation, massive early-type galaxies form late ( $z \approx 1 - 2$  depending on the cosmology) by agglomeration of smaller older sub-units, so the stars of the resulting elliptical are actually much older than the equilibrium morphology. Simulations (Kauffmann & Charlot 1998) suggest these scenarios can still explain the homogeneity of the early-type cluster galaxy population out to  $z \approx 0.9$  (e.g., Aragon-Salamanca et al. 1993; Kodama et al. 1998; Gladders et al. 1998; Stanford et al. 1998). However, it is at  $z \gtrsim 1$  when differences are predicted to become apparent, and there is little observational evidence in this regime due to the few number of  $z > 1$  clusters known. Spectroscopic follow-up of the remaining red galaxies in the 1213-0017 field combined with their *HST* images should prove very useful in addressing this issue.

## 5. Conclusions

We have found an overdensity of EROs in the field of the  $z = 2.69$  quasar QSO 1213–0017 (UM 485), about a factor of 16 overdense compared to the blank field ERO surface density and at least of factor of 6 overdense at the 95% confidence level. The optical/IR colors of the EROs and numerous other red galaxies in this field are consistent with those of passively-evolving elliptical galaxies at  $z > 1$ . *HST* optical imaging shows a few of the red ( $R - K > 5$ ) galaxies seem to have early-type morphologies while the remainder are either disk galaxies or diffuse objects without any obvious core. Their near-IR morphologies are consistent with those observed in the optical, unlike in the case of the prototypical ERO HR 10. This suggests that the dust extinction in these galaxies is either relatively smooth or that reddening by dust is not a significant cause of the colors.

Follow-up Keck spectroscopy has measured redshifts for five red galaxies. Four lie at  $z \approx 1.31$ ,

and three of these have rest-frame UV absorption-line spectra similar to present-day elliptical galaxies, making this the most distant concentration of old galaxies spectroscopically confirmed to date. Including an Mg II absorber seen in the spectrum of the background quasar, there are five spectroscopic redshifts at  $z \approx 1.31$  with a standard deviation of  $1800 \text{ km s}^{-1}$  and a full range of  $3800 \text{ km s}^{-1}$  in the mean rest frame.

A number of lines of evidence possibly suggest the red galaxies in this field delineate the presence of a massive high-redshift cluster. The ERO surface density is enhanced above blank field counts, and there are five spectroscopic redshifts close together. The reddest 1213–0017 galaxies, three of which have the spectra of early-type galaxies, are nearly as luminous and as red as the brightest Coma cluster ellipticals. The red galaxies also have a large angular extent on the sky, and a considerable velocity spread, suggesting dynamical youthfulness. An impression of youthfulness is also conveyed by the roughly filamentary distribution of the red galaxies on the sky.

Aside from the direct physical evidence, the presence of spectroscopically old EROs provides circumstantial support to the idea of a cluster. Elliptical galaxies in the local Universe, presumably the present-day counterparts of  $z > 1$  old EROs, are highly clustered and predominantly found in high density regions (e.g., Dressler 1980). Such an analogy suggests that old EROs should be found with others of their ilk — this idea has yet to be fully explored. Since the hallmark of rich clusters is the presence of old ellipticals, this  $z = 1.31$  field may be one of the most distant rich cluster candidates to date. Moreover, regardless of whether this system is shown to be a genuine massive cluster, the concentration of EROs is likely a sign that this field is an uncommonly overdense region at high redshift, which warrants follow-up studies.

Further observations are needed to develop a full physical picture of this field. A much larger sample of redshifts, inferred from multicolor photometric redshifts and directly measured from deep spectroscopy, will reveal the number of luminous galaxies at this redshift. An expanded spectroscopic sample will also be valuable to measure the galaxy velocity distribution and to search for dynamical sub-structure. X-ray observations will allow us to look for hot intracluster gas, a sign of a deep gravitational potential, and also for mass sub-structure. This issue can also be addressed with radio observations to search for a Sunyaev-Zeldovich decrement.

Extending galaxy cluster studies to  $z > 1$  has special importance since current hierarchical formation theories predict massive galaxies assemble from smaller sub-units during this epoch (e.g., Kauffmann & Charlot 1998), so we can potentially test these models by witnessing the formation process in situ. Measuring the high-redshift cluster abundance using wide-area surveys can provide strong tests of cosmological models (Eke et al. 1996; Bahcall et al. 1997). However, even before a large number of such clusters have been found, the few known to date are valuable sites to investigate the processes which drive the evolution of the oldest stellar populations, galaxies, and galaxy clusters. Furthermore, these clusters can also be used as testing grounds for  $z > 1$  cluster-search strategies, which by necessity are derived from extrapolating the known properties of lower-redshift clusters. It may be that we have to abandon some common precepts formed from studying

local rich clusters in order to develop a complete understanding of high-redshift clusters and their constituent galaxies at an epoch of less than half the current age of the Universe.

Much of the data presented herein were obtained at the W. M. Keck Observatory, which is operated as a scientific partnership among the California Institute of Technology, the University of California and the National Aeronautics and Space Administration. The Observatory was made possible by the generous financial support of the W. M. Keck Foundation. We are grateful to Hyron Spinrad, Aaron Barth, and Dave Burstein for discussions which improved this work. It is also a pleasure for us to acknowledge Rychard Bouwens for the stellar population model calculations, Adam Stanford for the redshifted Coma color-magnitude relation, Dave Thompson for results from the CADIS survey, and Jim Rose and Dave Burstein for providing UV spectra. We thank the NOAO staff for assistance with the Kitt Peak observing runs, and Greg Wirth, David Sprayberry, and Ron Quick for supporting the Keck/LRIS observations. Dan Stern and Andy Bunker provided helpful advice and software for the LRIS reductions. We also thank Emmanuel Bertin for distributing SExtractor, and Wayne Landsman and Jonathan Baker for contributing IDL routines. Jenny Graves helped with the initial near-IR reductions and photometry. This research has made use of the Digitized Sky Survey, NASA’s Astrophysics Data System Abstract Service, and the NASA/IPAC Extragalactic Database (NED). A. Dey acknowledges financial support from NASA grant HF-01089.01-97A. This work has also received support from *HST* NASA grant GO-06958.02-95A.

## REFERENCES

Aragon-Salamanca, A., Ellis, R. S., Couch, W. J., & Carter, D. 1993, MNRAS, 262, 764

Bahcall, N. A., Fan, X., & Cen, R. 1997, ApJ, 485, L53

Barger, A. J., Cowie, L. L., Trentham, N., Fulton, E., Hu, E. M., Songaila, A., & Hall, D. 1999, AJ, 117, 102

Beckwith, S. V. W., Thompson, D., Mannucci, F., & Djorgovski, S. G. 1998, ApJ, 504, 107

Beers, T. C., Flynn, K., & Gebhardt, K. 1990, AJ, 100, 32

Bershady, M. A., Lowenthal, J. D., & Koo, D. C. 1998, ApJ, 505, 50

Bertin, E. & Arnouts, S. 1996, A&AS, 117, 393

Brown, T. M., Ferguson, H. C., Deharveng, J.-M., & Jedrzejewski, R. I. 1998, ApJ, 508, L139

Casali, M. M. & Hawarden, T. G. 1992, JCMT-UKIRT Newsletter, 4, 33

Charlton, J. C. & Churchill, C. W. 1996, ApJ, 465, 631

Cimatti, A., Andreani, P., Rottgering, H., & Tilanus, R. 1998, Nature, 392, 895

Clowe, D., Luppino, G. A., Kaiser, N., Henry, J. P., & Gioia, I. M. 1998, *ApJ*, 497, L61

Cohen, J. G., Blandford, R., Hogg, D. W., Pahre, M. A., & Shopbell, P. L. 1999, *ApJ*, 512, 30

Coleman, G. D., Wu, C. C., & Weedman, D. W. 1980, *ApJS*, 43, 393

Cowie, L. L., Gardner, J. P., Hu, E. M., Songaila, A., Hodapp, K. W., & Wainscoat, R. J. 1994, *ApJ*, 434, 114

Dey, A., Graham, J. R., Ivison, R. J., Smail, I., Wright, G. S., & Liu, M. C. 1999, *ApJ*, 519, 610

Dey, A., Spinrad, H., & Dickinson, M. 1995, *ApJ*, 440, 515

Dey, A. et al. 2000, in preparation

Dickinson, M. 1995, in *ASP Conf. Series*, Vol. 86, *Fresh Views of Elliptical Galaxies*, ed. A. Buzzoni, A. Renzini, & A. Serrano, 283

Dickinson, M. 1997, in *Galaxy Scaling Relations: Origins, Evolution and Applications*, ed. L. N. da Costa & A. Renzini, *ESO Astrophysics Symposia* (Springer), 215 (astro-ph/9703035)

Dickinson, M. & Steidel, C. C. 1996, in *IAU Symposium*, Vol. 171, *New Light on Galaxy Evolution*, ed. R. Bender & R. L. Davies (Kluwer), 295

Djorgovski, S., Soifer, B. T., Pahre, M. A., Larkin, J. E., Smith, J. D., Neugebauer, G., Smail, I., Matthews, K., Hogg, D. W., Blandford, R. D., Cohen, J., Harrison, W., & Nelson, J. 1995, *ApJ*, 438, L13

Dressler, A. 1980, *ApJ*, 236, 351

Dunlop, J. 1998, in *KNAW Colloquium: The Most Distant Radio Galaxies*, ed. P. N. Best et al. (Reidel), in press (astro-ph/9801114)

Dunlop, J., Peacock, J., Spinrad, H., Dey, A., Jimenez, R., Stern, D., & Windhorst, R. 1996, *Nature*, 381, 581

Eisenhardt, P. & Dickinson, M. 1992, *ApJ*, 399, L47

Eke, V. R., Cole, S., & Frenk, C. S. 1996, *MNRAS*, 282, 263

Elston, R., Rieke, G. H., & Rieke, M. J. 1988, *ApJ*, 331, L77

Elston, R., Rieke, M. J., & Rieke, G. H. 1989, *ApJ*, 341, 80

Fanelli, M. N., O'Connell, R. W., Burstein, D., & Wu, C. C. 1990, *ApJ*, 364, 272

—. 1992, *ApJS*, 82, 197

Gioia, I. M., Henry, J. P., Mullis, C. R., Ebeling, H., & Wolter, A. 1999, *AJ*, 117, 2608

Gladders, M. D., Lopez-Cruz, O., Yee, H. K. C., & Kodama, T. 1998, *ApJ*, 501, 571

Graham, J. R. & Dey, A. 1996, *ApJ*, 471, 720

Graham, J. R., Matthews, K., Soifer, B. T., Nelson, J. E., Harrison, W., Jernigan, J. G., Lin, S., Neugebauer, G., Smith, G., & Ziolkowski, C. 1994, *ApJ*, 420, L5

Hall, P. B. & Green, R. F. 1998, *ApJ*, 507, 558

Hall, P. B., Green, R. F., & Cohen, M. 1998, *ApJS*, 119, 1

Hammer, F., Flores, H., Lilly, S. J., Crampton, D., Le Fevre, O., Rola, C., Mallen-Ornelas, G., Schade, D., & Tresse, L. 1997, *ApJ*, 481, 49

Heap, S. R., Brown, T. M., Hubeny, I., Landsman, W., Yi, S., Fanelli, M., Gardner, J. P., Lanz, T., Maran, S. P., Sweigart, A., Kaiser, M. E., Linsky, J., Timothy, J. G., Lindler, D., Beck, T., Bohlin, R. C., Clampin, M., Grady, J., Loiacono, J., & Krebs, C. 1998, *ApJ*, 492, L131

Henry, J., Gioia, I., Mullis, C., Clowe, D., Luppino, G., Boehringer, H., Briel, U., Voges, W., & Huchra, J. 1997, *AJ*, 114, 1293

Hu, E. M. & Ridgway, S. E. 1994, *AJ*, 107, 1303

Kauffmann, G. & Charlot, S. 1998, *MNRAS*, 294, 705

Kauffmann, G., Charlot, S., & White, S. D. M. 1996, *MNRAS*, 283, L117

Kennicutt, R. C., J. 1983, *ApJ*, 272, 54

Kennicutt, Robert C., J. 1992, *ApJ*, 388, 310

Kinney, A. L., Calzetti, D., Bohlin, R. C., McQuade, K., Storchi-Bergmann, T., & Schmitt, H. R. 1996, *ApJ*, 467, 38

Kodama, T., Arimoto, N., Barger, A. J., & Arag'On-Salamanca, A. 1998, *A&A*, 334, 99

Kotilainen, J. K. & Ward, M. J. 1994, *MNRAS*, 266, 953

Kron, R. G. 1980, *ApJS*, 43, 305

Lanzetta, K. M., Wolfe, A. M., & Turnshek, D. A. 1987, *ApJ*, 322, 739

Lilly, S. J., Gardner, J. P., Cowie, L. L., & McLean, I. S. 1988, *ApJ*, 332, L59

Liu, M. C., Dey, A., Graham, J. R., Steidel, C. C., & Adelberger, K. A. 1999, in *The Hy-Redshift Universe: Galaxy Formation and Evolution at High-Redshift*, ed. A. J. Bunker & W. J. H. van Breugel, ASP Conf. Series, in press (astro-ph/9910434)

Lubin, L. M., Postman, M., & Oke, J. B. 1998, *AJ*, 116, 643

Massey, P. & Gronwall, C. 1990, *ApJ*, 358, 344

Massey, P., Strobel, K., Barnes, J. V., & Anderson, E. 1988, *ApJ*, 328, 315

Matthews, K. & Soifer, B. 1994, in *Infrared Astronomy with Arrays: The Next Generation*, ed. I. McLean (Dordrecht: Kluwer), 239

McCarthy, P. J., Persson, S. E., & West, S. C. 1992, *ApJ*, 386, 52

McCracken, H. J., Metcalfe, N., Shanks, T., Campos, A., Gardner, J. P., & Fong, R. 2000, *MNRAS*, 311, 707

McLeod, B. A., Bernstein, G. M., Rieke, M. J., Tollestrup, E. V., & Fazio, G. G. 1995, *ApJS*, 96, 117

Morton, D. C., Bruzual A., G., Kurucz, R. L., & Spinrad, H. 1977, *ApJ*, 212, 438

O'Connell, R. W. 1999, *ARAA*, 37, 603

Oke, J. B., Cohen, J. G., Carr, M., Cromer, J., Dingizian, A., Harris, F. H., Labrecque, S., Lucinio, R., Schaal, W., Epps, H., & Miller, J. 1995, *PASP*, 107, 375

Oke, J. B. & Gunn, J. E. 1983, *ApJ*, 266, 713

Peacock, J. A., Jimenez, R., Dunlop, J. S., Waddington, I., Spinrad, H., Stern, D., Dey, A., & Windhorst, R. A. 1998, *MNRAS*, 296, 1089

Persson, S. E., Murphy, D. C., Krzeminski, W., Roth, M., & Rieke, M. J. 1998, *AJ*, 116, 2475

Ponder, J. M., Burstein, D., O'Connell, R. W., Rose, J. A., Frogel, J. A., Wu, C. C., Crenshaw, D. M., Rieke, M. J., & Tripicco, M. 1998, *AJ*, 116, 2297

Postman, M., Lubin, L. M., & Oke, J. B. 1998, *AJ*, 116, 560

Rosati, P., Stanford, S. A., Eisenhardt, P. R., Elston, R., Spinrad, H., Stern, D., & Dey, A. 1999, *AJ*, in press (astro-ph/9903381)

Rose, J. A. & Deng, S. 1999, *AJ*, 117, 2213

Schade, D., Lilly, S. J., et al. 1999, *AJ*, in press (astro-ph/9906171)

Schlegel, D. J., Finkbeiner, D. P., & Davis, M. 1998, *ApJ*, 500, 525

Smail, I., Ivison, R. J., Blain, A. W., & Kneib, J.-P. 1998, *ApJ*, 507, L21

Smail, I., Ivison, R. J., Kneib, J.-P., Cowie, L. L., Blain, A. W., Barger, A. J., Owen, F. N., & Morrison, G. E. 1999, *MNRAS*, in press (astro-ph/9905246)

Soifer, B. T., Matthews, K., Djorgovski, S., Larkin, J., Graham, J. R., Harrison, W., Jernigan, G., Lin, S., Nelson, J., Neugebauer, G., Smith, G., Smith, J. D., & Ziolkowski, C. 1994, *ApJ*, 420, L1

Soifer, B. T., Matthews, K., Neugebauer, G., Armus, L., Cohen, J. G., Persson, S. E., & Smail, I. 1999, *AJ*, in press (astro-ph/9906464)

Spinrad, H., Dey, A., Stern, D., Dunlop, J., Peacock, J., Jimenez, R., & Windhorst, R. 1997, *ApJ*, 484, 581

Stanford, S. A., Eisenhardt, P. R., & Dickinson, M. 1998, *ApJ*, 492, 461

Stanford, S. A., Elston, R., Eisenhardt, P. R., Spinrad, H., Stern, D., & Dey, A. 1997, *AJ*, 114, 2232

Steidel, C. C. 1993, in *The Environment and Evolution of Galaxies*, ed. J. M. Shull & H. A. Thronson (Kluwer), 263

Steidel, C. C. 1995, in *QSO Absorption Lines*, ed. G. Meylan (Springer), 139 (astro-ph/9509098)

Steidel, C. C. & Dickinson, M. 1995, in *Wide Field Spectroscopy and the Distant Universe: The 35th Herstmonceux Conference*, ed. S. J. Maddox & A. Aragon-Salamanca (World Scientific), in press (astro-ph/9409061)

Steidel, C. C. & Hamilton, D. 1993, *AJ*, 105, 2017

Steidel, C. C. & Sargent, W. L. W. 1992, *ApJS*, 80, 1

Stern, D., Dey, A., Spinrad, H., Maxfield, L., Dickinson, M., Schlegel, D., & González, R. A. 1999, *AJ*, 117, 1122

Teplitz, H. I., Malkan, M., & McLean, I. S. 1998, *ApJ*, 506, 519

Thompson, D., Beckwith, S. V. W., Fockenbrock, R., Fried, J., Hippelein, H., Huang, J. S., Von Kuhlmann, B., Leinert, C., Meisenheimer, K., Phleps, S., Röser, H. J., Thommes, E., & Wolf, C. 1999, *ApJ*, 523, 100

Thompson, D., Mannucci, F., & Beckwith, S. V. W. 1996, *AJ*, 112, 1794

Tonry, J. & Davis, M. 1979, *AJ*, 84, 1511

Trentham, N., Kormendy, J., & Sanders, D. B. 1999, *AJ*, 117, 2152

Wu, C. C. et al. 1991, *IUE Newsletter*, 84

Yi, S., Brown, T. M., Heap, S., Hubeny, I., Landsman, W., Lanz, T., & Sweigart, A. 1999a, *ApJ*, in press (astro-ph/9911067)

Yi, S., Lee, Y. W., Woo, J. H., Park, J. H., Demarque, P., & Oemler, A., J. 1999b, ApJ, 513, 128

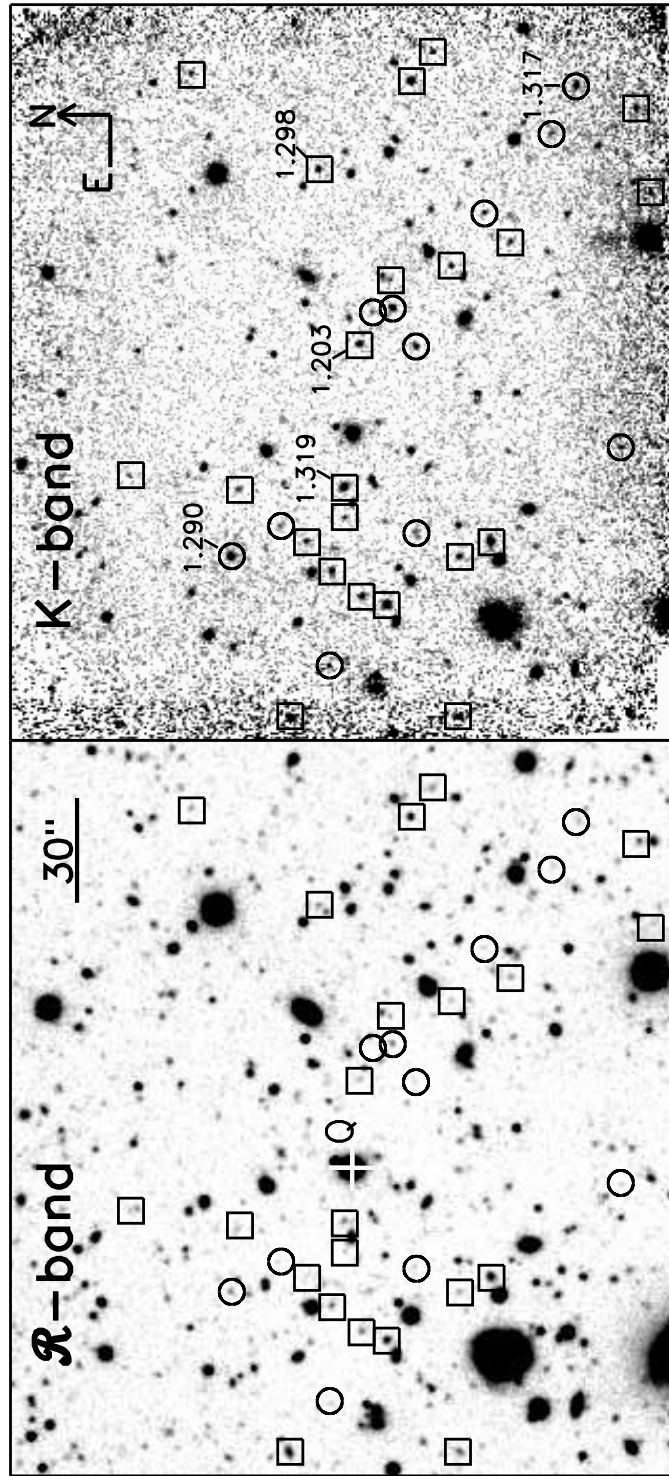


Fig. 1.— KPNO  $\mathcal{R}$  and  $K$ -band images of the 1213–0017 field. Each is  $3'5 \times 3'1$ . Objects with  $\mathcal{R} - K > 6$  are circled (○) and those with  $\mathcal{R} - K = 5 - 6$  are marked with a square (□). The quasar is marked on the  $\mathcal{R}$ -band image with a white cross and labelled “Q”. Red galaxies with spectroscopic redshifts are labelled.

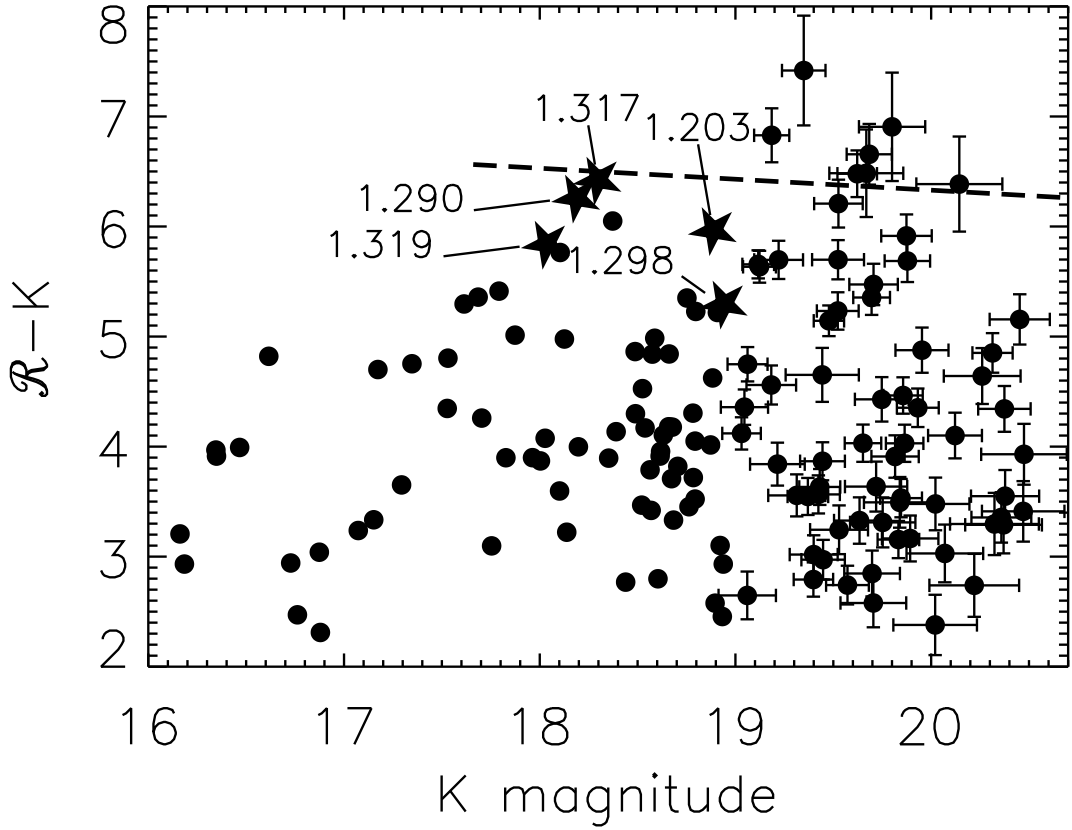


Fig. 2.— Color-magnitude diagram for objects detected in the 11 arcmin<sup>2</sup>  $K$ -band image shown in Fig. 1. The error bars for  $K < 19$  objects are smaller than the plotting symbols.  $\mathcal{R}$ -band magnitudes are AB-based, and  $K$ -band mags are Vega-based. There are 11 objects with  $\mathcal{R} - K > 6$  and another 22 with  $\mathcal{R} - K = 5 - 6$ . The dashed line represents a no-evolution color-magnitude locus for elliptical galaxies at  $z = 1.3$  based on Coma cluster galaxies (Stanford et al. 1998), with the bright end indicating the expected location of the brightest cluster galaxy. The stars ( $\star$ ) show the five objects with spectroscopic redshifts.

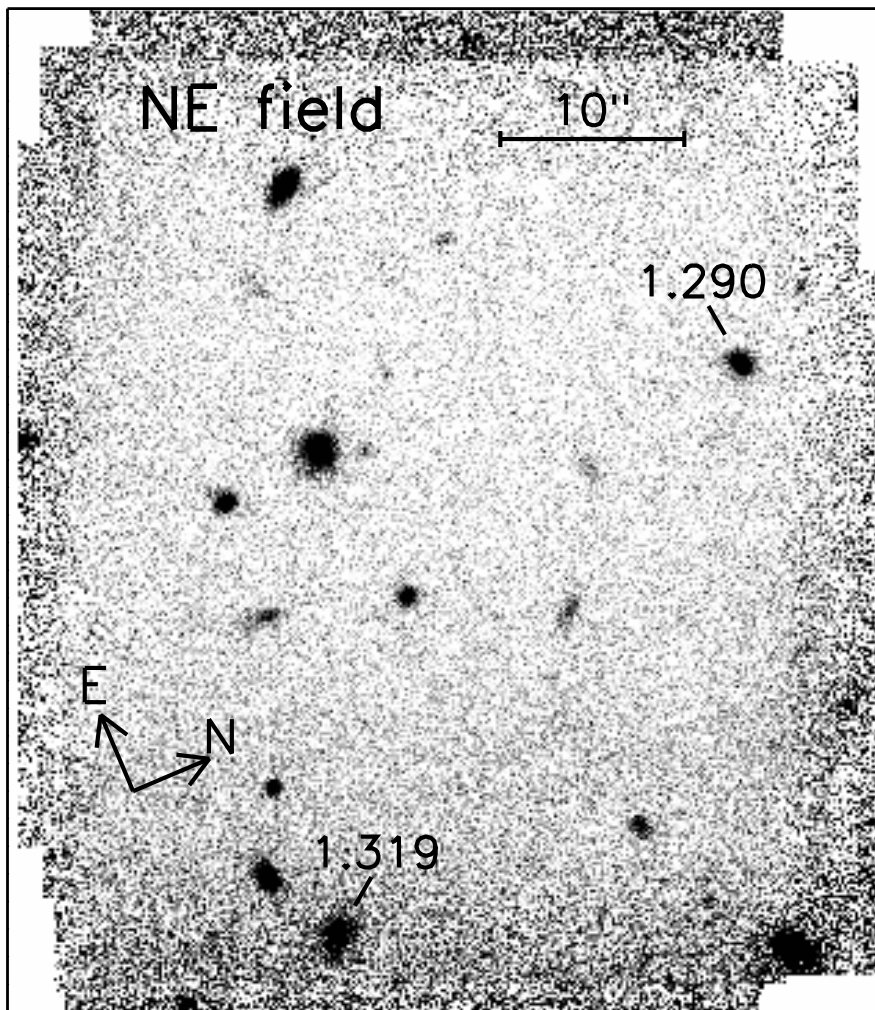


Fig. 3.— Keck  $K$ -band image of a field NE of QSO 1213-0017 (see § 2.2.2 for position) shown with a linear stretch. The field is  $47'' \times 55''$ . The very faintest objects in the images are  $K \approx 20.5$  mag. EROs with spectroscopic redshifts are labeled.

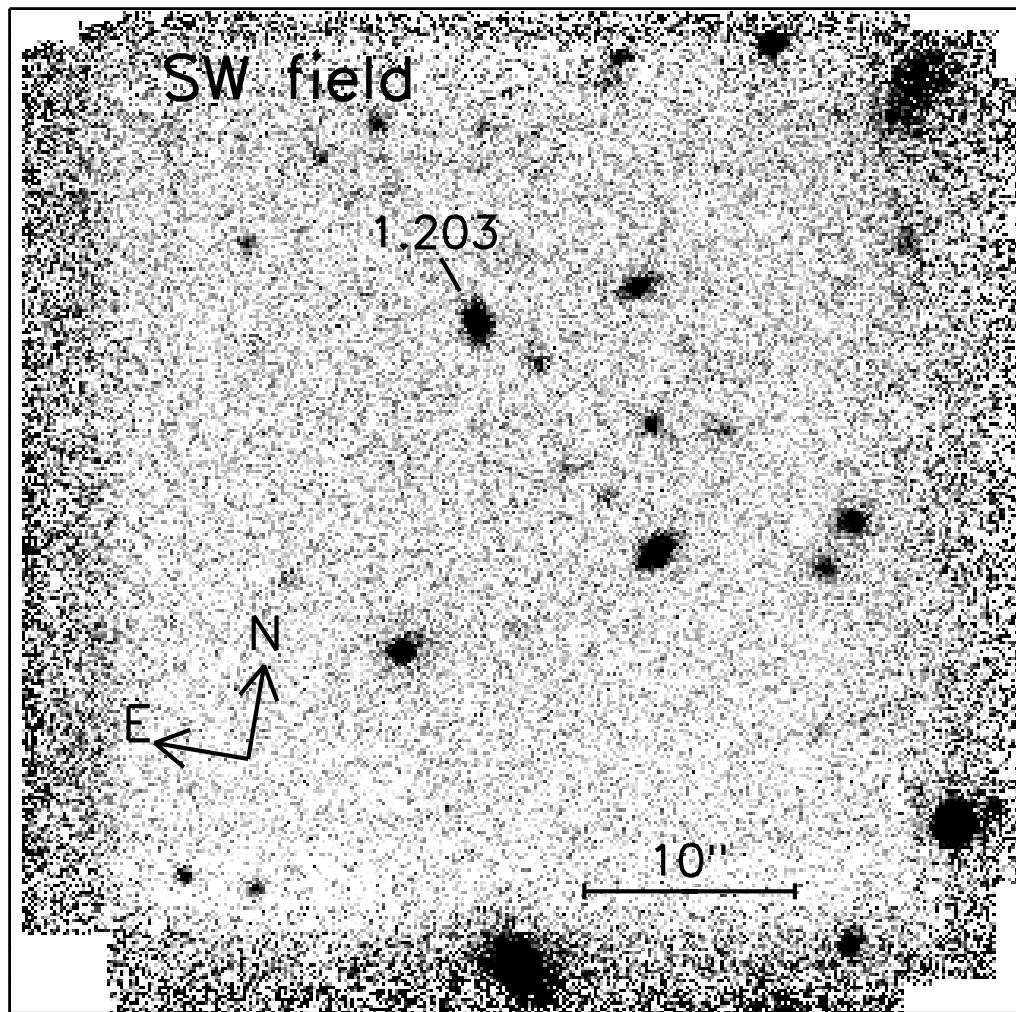


Fig. 4.— Keck  $K$ -band image of a field SW of QSO 1213-0017 (see § 2.2.2 for position) shown with a linear stretch. The field is  $48'' \times 48''$ . The very faintest objects in the images are  $K \approx 21.3$  mag. The one EROs in the image with a spectroscopic redshift is labeled.

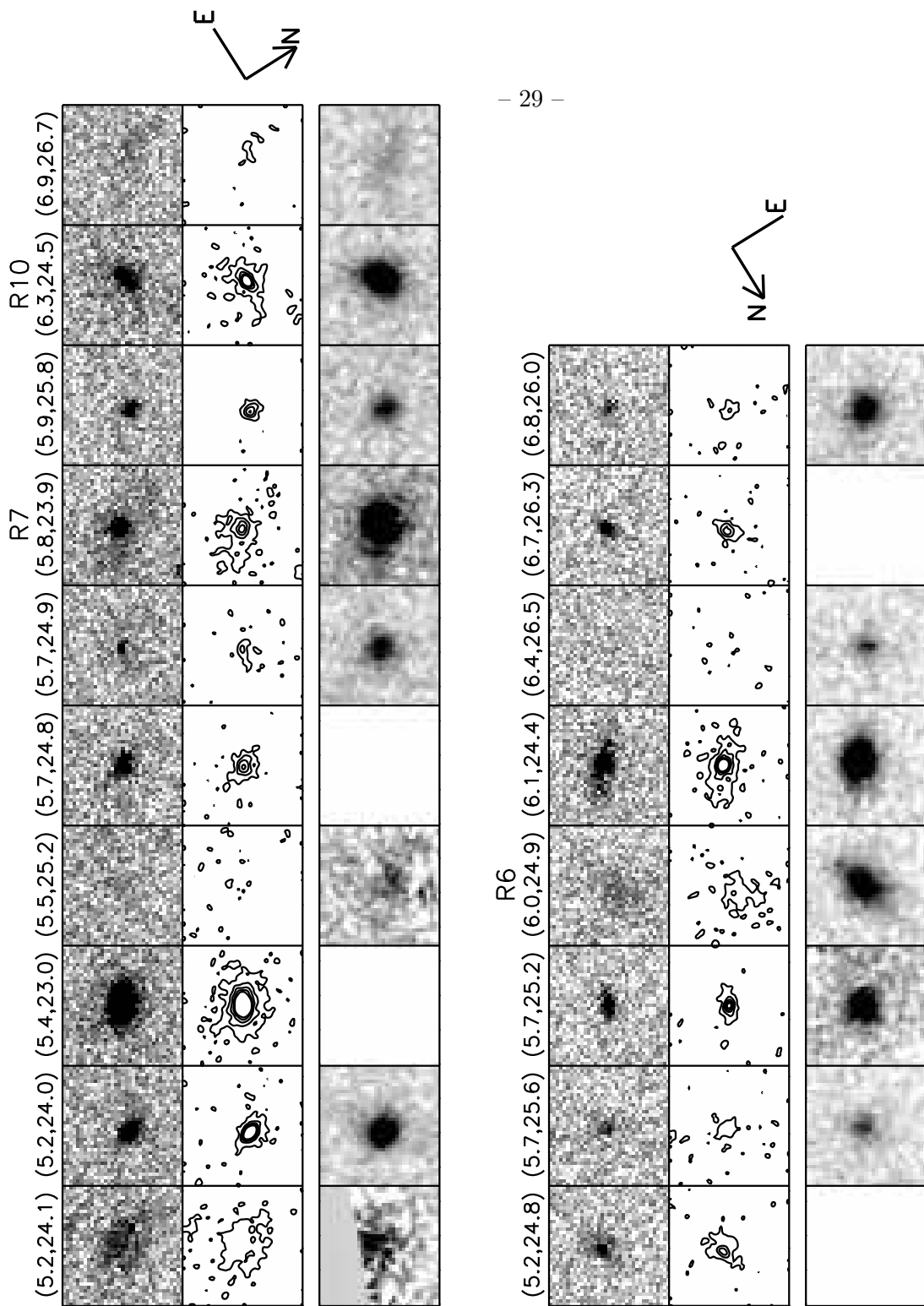


Fig. 5.— *HST F814W* and *Keck K-band* images for most of the red galaxies in the field of QSO 1213-0017. The top set is from WF3, which covers the field NE of the quasar, and the bottom set from WF4, covering the SW field. For each set, the top row shows the greyscale *HST* image, the middle row shows contours for the *HST* data drawn at  $\{\frac{1}{4}, \frac{3}{4}, \frac{5}{4}, \frac{7}{4}, \frac{9}{4}\} \times \sigma$ , and the bottom row shows the *Keck* image, when available. The orientation on the sky is shown at the right edge of each set. The images are  $3.5''$  ( $30 h_{50}^{-1}$  kpc) on a side and displayed with a linear stretch. The  $R - K$  color and  $R$  mag measured from our KPNO data are above each object. The three with redshifts (R6, R7, and R10) are labeled. Most of the red galaxies have a regular appearance, and none are obviously interacting or disturbed.

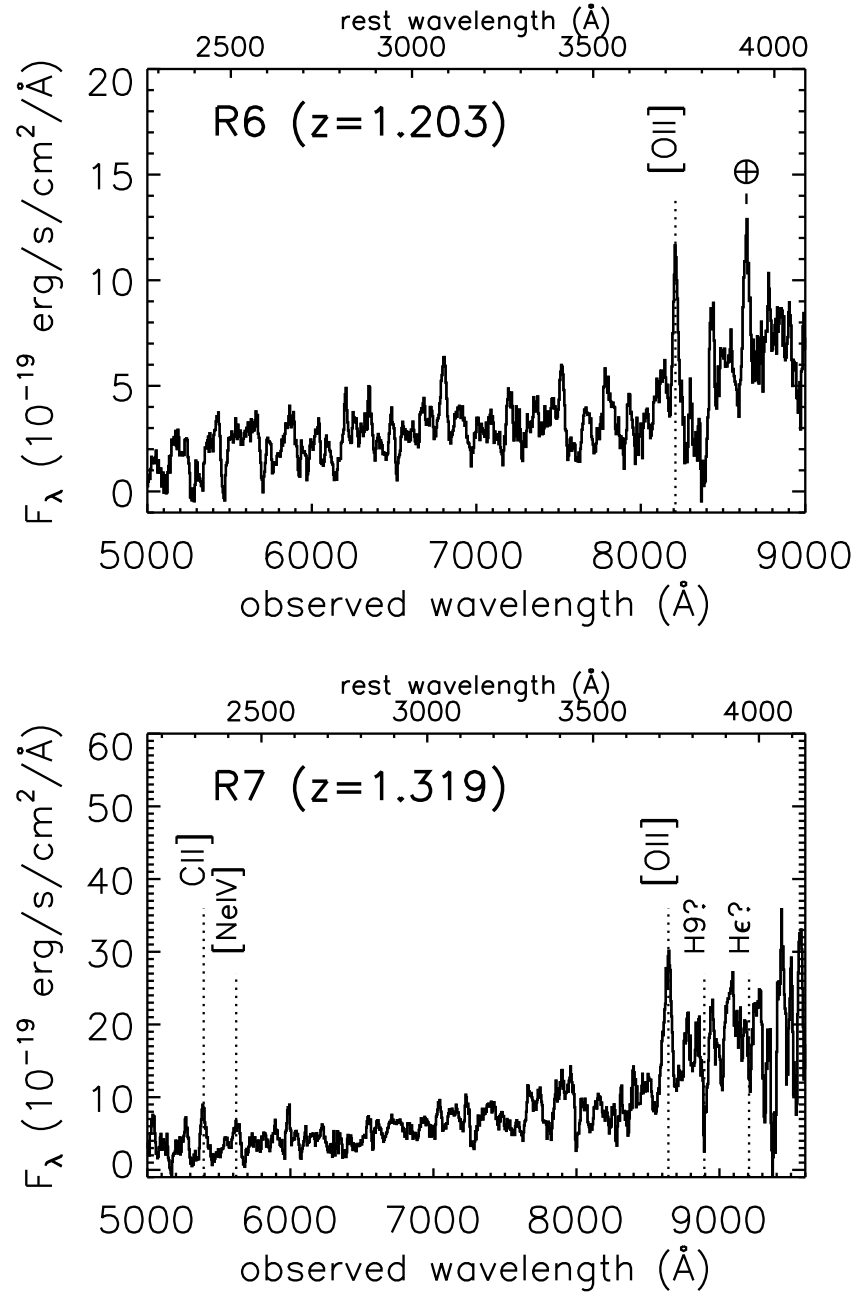


Fig. 6.— Keck/LRIS spectrum of two emission-line red galaxies. Both spectra have been smoothed with a boxcar filter of width 7 pixels. **Top:** R6 shows a single strong emission line at 8210 Å, which we assume is [O II]  $\lambda 3727$ . The feature at 8642 Å is due to imperfect cancellation of a CCD fringe from a strong sky line. **Bottom:** R7 shows emission lines of C II]  $\lambda 2326$  and [O II]  $\lambda 3727$ , and also a weak [Ne IV]  $\lambda 2424$  line close to the telluric [O I] line at 5577 Å.

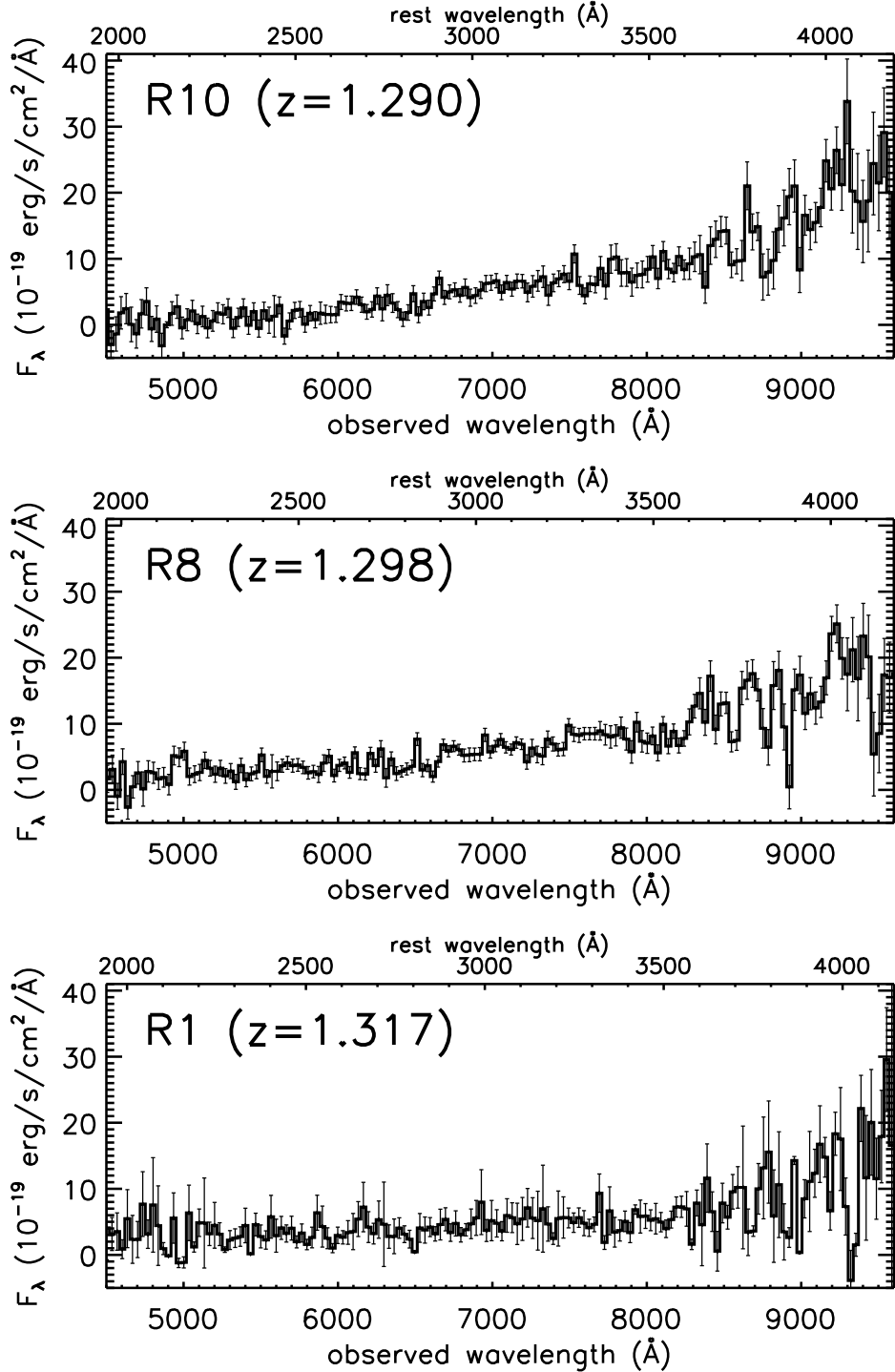


Fig. 7.— Keck/LRIS spectrum of the three absorption-line red galaxies. The spectra have been averaged in 7 pixel bins with the formal  $1\sigma$  errors overlaid. See the text and later figures for a description of the redshift determination. At  $\lambda \gtrsim 8500$  Å, the noise of the spectra increases due to telluric OH emission lines and also imperfect removal of CCD fringes.

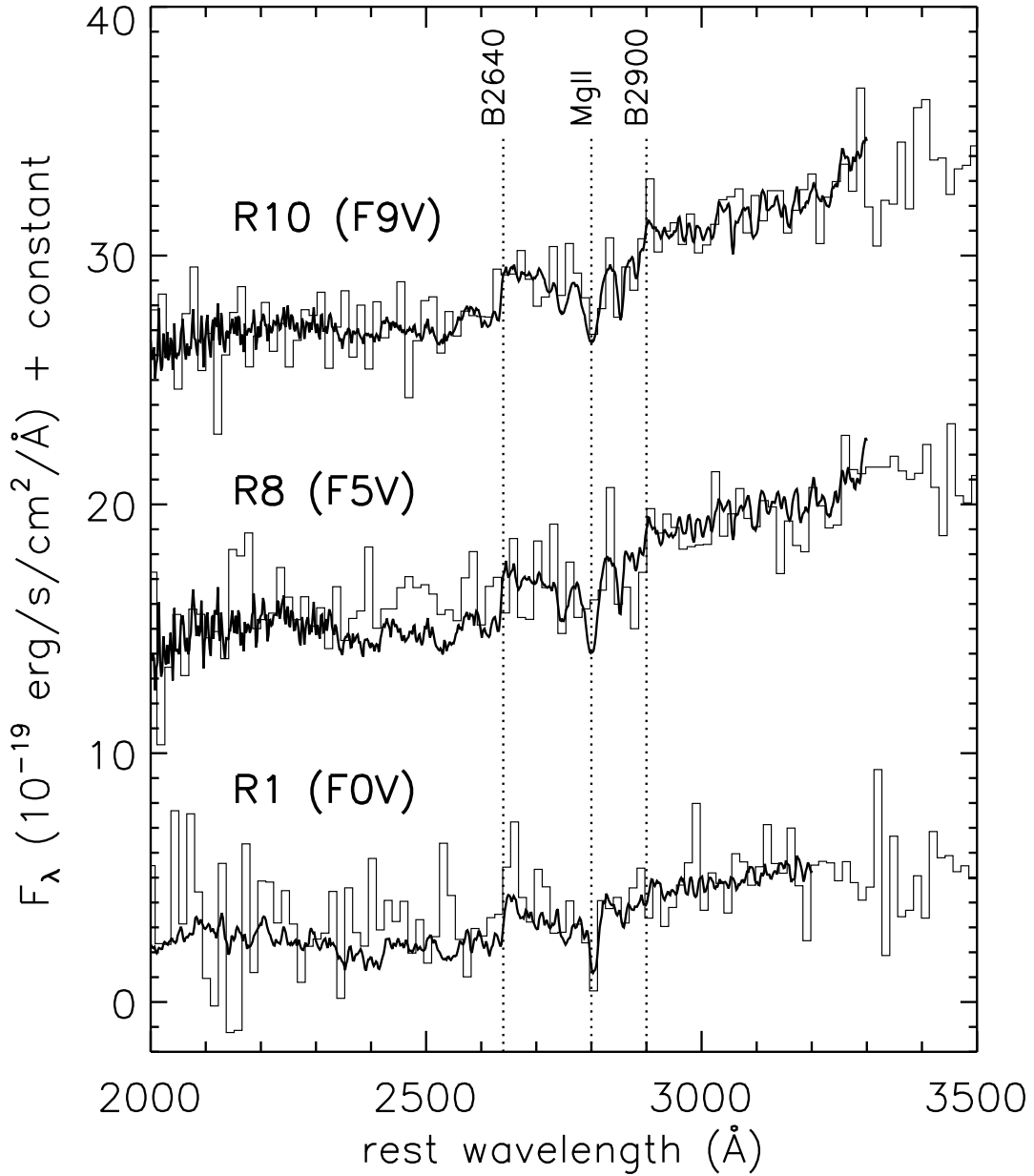


Fig. 8.— Rest-frame UV spectra of the three continuum-break galaxies, averaged in 7 pixel bins. The R8 spectrum is offset by +13 along the y-axis and the R10 spectrum by +26. Overplotted with the thick lines are *IUE* spectra of dwarfs. The *IUE* spectra have been normalized to the galaxy flux longward of 3000 Å; notice the good agreement between the star and galaxy spectra all the way to the bluest wavelengths. This suggests the amount of any ongoing or recent star formation, which would be revealed by a rising blue continuum, is small.

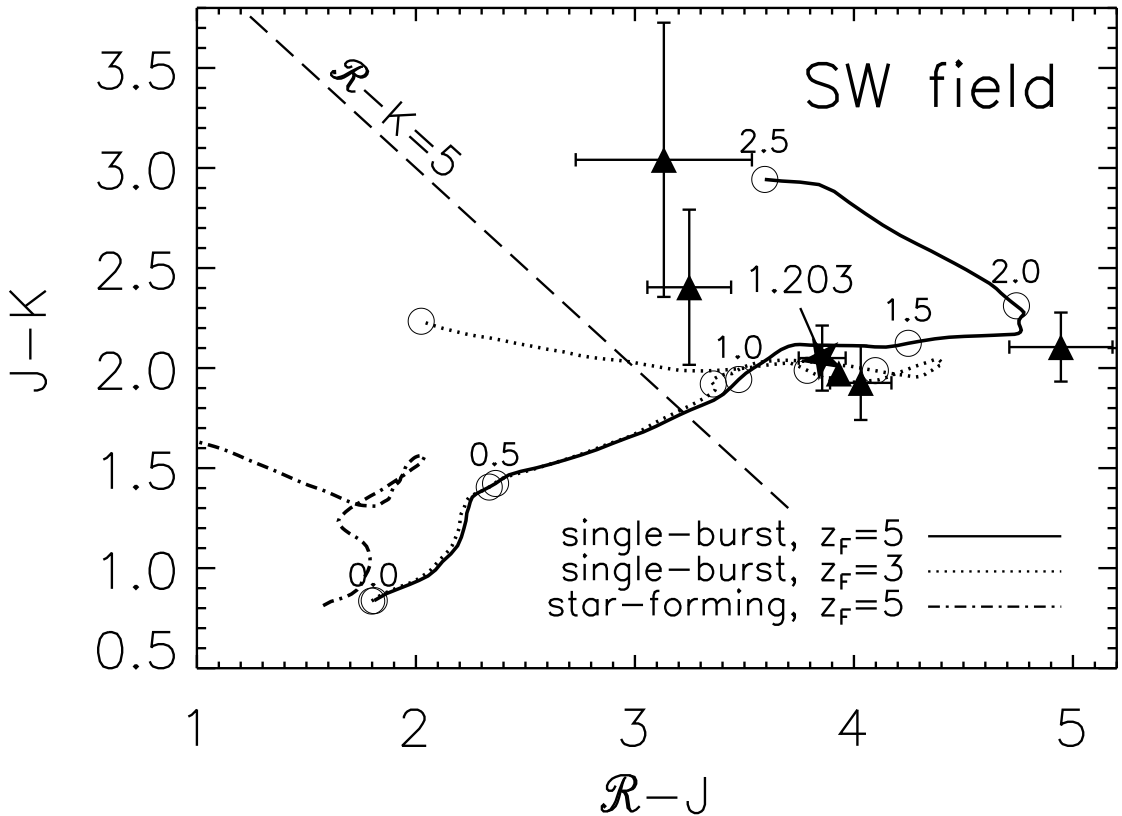


Fig. 9.—  $\mathcal{R}JK$  color-color plot of red ( $\mathcal{R} - K > 5$ ) objects in the Keck/NIRC field SW of the quasar, the only field with IR photometry in two filters. The data point without error bars has errors comparable to its symbol size. Overplotted are single-burst models of Bruzual & Charlot (1996) passively evolving from formation redshifts of  $z_F = 3$  and 5. The open circles ( $\circ$ ) show the observed model colors at  $z = 0 - 2.5$ . The colors of the single-burst models diverge for  $z \gtrsim 1.5$ . We also plot colors for an exponentially decaying star-forming model with an  $e$ -folding time of 6 Gyr, which well reproduces the colors of local spiral galaxies (e.g., Charlot & Bruzual 1991); its colors never become significantly red. The observed colors of the well-detected red galaxies suggest these objects lie at  $z = 1 - 2$ , corroborating the color-magnitude plot in Figure 2. The object marked with a star ( $\star$ ) is R6, an emission-line ERO at  $z = 1.203$ .

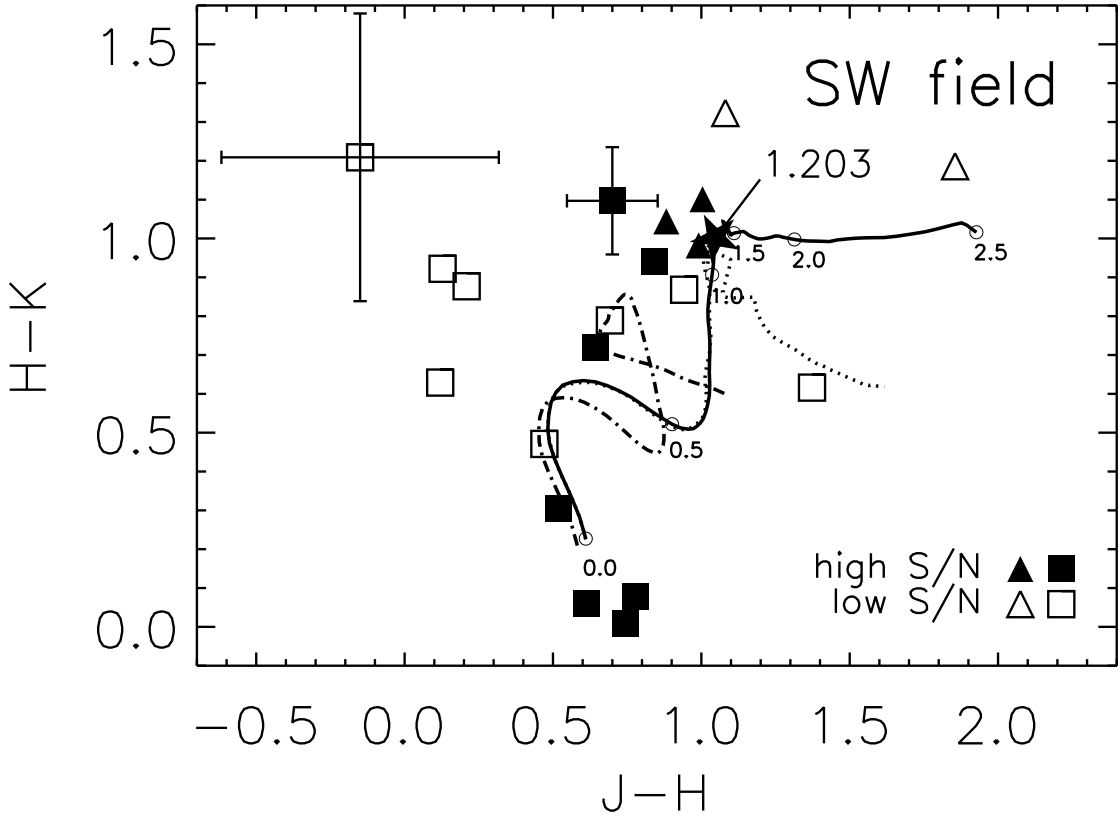


Fig. 10.—  $JHK$  color-color plot for all objects in the Keck/NIRC images SW of the quasar, the only field where we measured two IR colors. The filled symbols are the data with errors in both colors of  $\leq 0.25$  mag, and the empty symbols are the lower S/N data. The triangles indicate the  $R - K > 5$  objects from Figure 9. The median errors for each subset are plotted on one data point. The lines show the same theoretical models as in Figure 9. The observed colors of the well-detected red galaxies suggest these objects lie at  $z = 1 - 2$ . The one object in the field with a redshift, the emission-line ERO R6 at  $z = 1.203$ , is marked with a star (\*) and labeled.

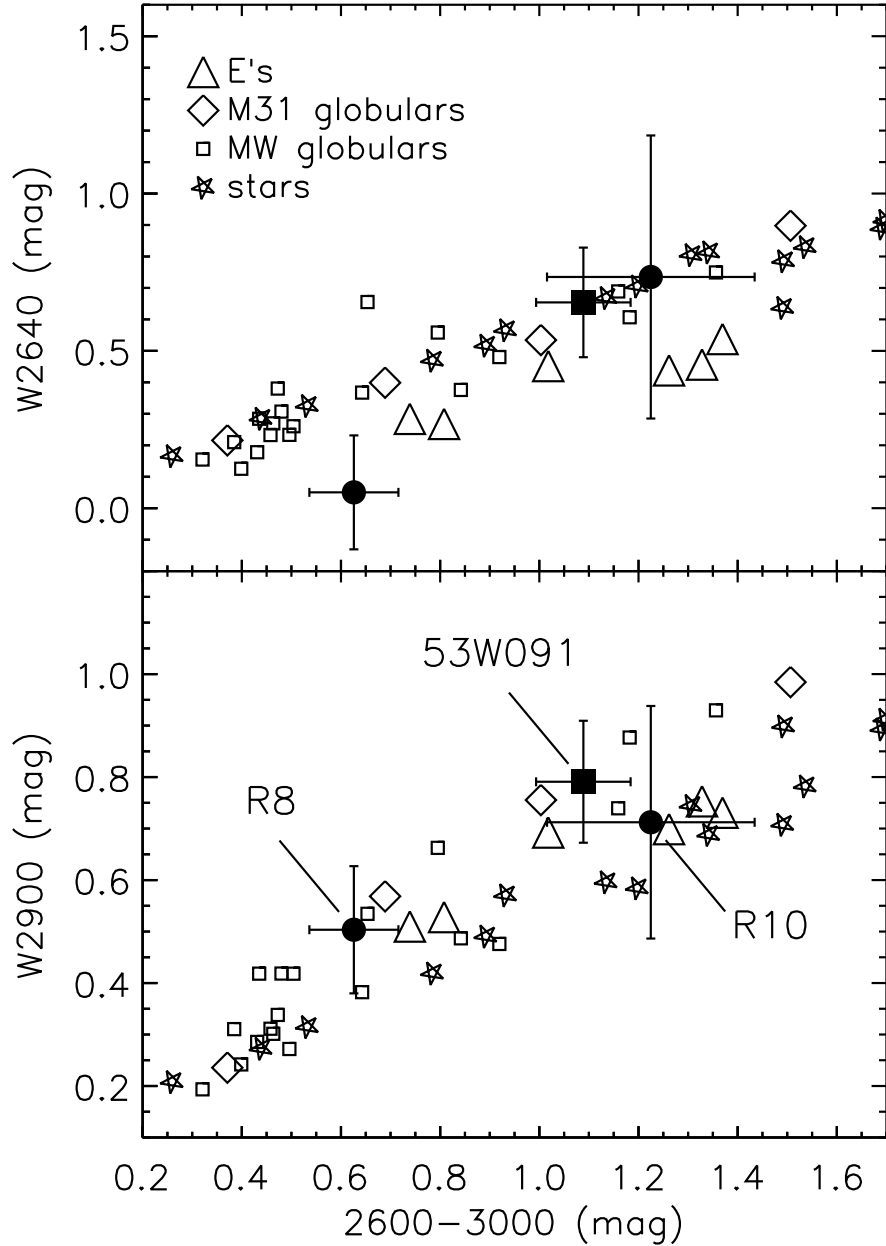


Fig. 11.— Strength of the UV-continuum breaks of red galaxies R8 and R10 compared with local old stellar populations and LBDS 53W091 at  $z = 1.55$ . W2640 and W2900 measure the 2640 Å and 2900 Å breaks, respectively, and 2600 – 3000 is a moderate-bandwidth UV color. Data for individual stars are from Fanelli et al. (1992), for Milky Way globulars from Rose & Deng (1998), and for M 31 globulars and ellipticals from Ponder et al. (1998). More metal-poor globulars lie to the lower left and more metal-rich ones to the upper right. R8 is more similar to the more metal-poor local systems than R10. The W2640 offset between the M31 globular clusters and the local ellipticals is believed to arise from the UV-excess population in the ellipticals.

Table 1. Spectroscopic Redshifts in the 1213–0017 Field

Identification	RA (J2000)	Dec (J2000)	$K$ (mag)	$\mathcal{R} - K$ (mag) <sup>a</sup>	Morphology <sup>b</sup>	$z$	Spectral Features
R1	12 15 43.2	−00 35 39	$18.30 \pm 0.07$	$6.42 \pm 0.15$	—	$1.317 \pm 0.005$	B2640, Mg II, B2900
R6	12 15 48.1	−00 34 37	$18.89 \pm 0.07$	$5.96 \pm 0.12$	diffuse <sup>c</sup>	$1.203 \pm 0.002$	[O II]
R7	12 15 50.9	−00 34 32	$18.04 \pm 0.04$	$5.84 \pm 0.07$	compact+disk?	$1.319 \pm 0.002$	[O II], C II], [Ne IV], C III]?
R8	12 15 44.8	−00 34 25	$18.94 \pm 0.09$	$5.30 \pm 0.13$	—	$1.298 \pm 0.004$	B2640, Mg II?, B2900, D4000?
R10	12 15 52.2	−00 34 00	$18.19 \pm 0.05$	$6.26 \pm 0.08$	edge-on disk	$1.290 \pm 0.002$	B2640, Mg II, B2900, D4000?
Mg II absorption <sup>d</sup>	12 15 49.8	−00 34 34				1.3196	
						1.5534	

<sup>a</sup> $\mathcal{R}$ -band mags are on the AB system while  $K$ -band mags are normalized to Vega (see § 2.1). A flat spectrum ( $f_\nu = \text{constant}$ ) source has  $\mathcal{R} - K = 1.85$ .

<sup>b</sup>Morphologies from our *HST F814W* images. Sources with a blank line “—” were not observed.

<sup>c</sup>Unlike the other EROs, which have similar morphologies in the *F814W* and  $K$ -band images, R6 appears diffuse in *F814W* but compact in the  $K$ -band images. See § 4.2.1 and Figure 5.

<sup>d</sup>From Steidel & Sargent (1992).

Table 2. Rest-Frame UV Spectral Indices

Name	Blue Passband (Å)	Red Passband (Å)	Definition	R8	R10
2600 – 3000	2470–2670	2930–3130	Fanelli et al. (1990)	$0.63 \pm 0.09$	$1.22 \pm 0.21$
2609/2660	2596–2623	2647–2673		$0.41 \pm 0.34$	$0.62 \pm 0.61$
2828/2921	2818–2838	2906–2936		$0.41 \pm 0.31$	$0.29 \pm 0.36$
W2640	2550–2625	2647–2722	this work	$0.05 \pm 0.18$	$0.73 \pm 0.45$
W2900	2773–2873	2910–3010		$0.50 \pm 0.12$	$0.71 \pm 0.23$